Applied Physics Laboratory
University of Washington

1013 NE 40th Street
Box 355640
Seattle, WA 98105-6698

206-543-1300
FAX 206-543-6785
www.apl.washington.edu

12 September 2013

To: Dr. Robert H. Headrick
Office of Naval Research (ONR 322)
875 N. Randolph Street, Suite 1425
Arlington, VA 22203-1995

From: Brian Todd Hefner

Subj: ONR Grant: N00014-10-1-0089
"The effects of sand sediment volume heterogeneities on sound propagation and scattering"

Encl: (1) Final Report for "The effects of sand sediment volume heterogeneities on sound propagation and scattering" with accompanying SF 298.
(2) In preparation publication to JASA: "Attenuation in Sand Sediments Due to Scattering from Porosity Fluctuations."
(3) ECUA 2010 Istanbul Proceedings: "Measurement and modeling of sound propagation in a heterogenous sediment."
(4) ECUA 2010 Istanbul Proceedings: "High frequency measurements of backscattering from heterogeneities and discrete scatterers in sand sediments."
(5) ECUA 2012 Edinburgh Proceedings: "Power-Law Attenuation Due to Scattering from Porosity Heterogeneities in Sandy Sediments."
(6) List of supported publications.

Enclosed please find the Final Report and corresponding SF 298 form (1) for the subject grant. Enclosures (2) through (5) are other articles and presentations; enclosure (6) is a listing of publications. These documents constitute the Final Technical Report and deliverables for ONR Grant N00014-10-1-0089.

Brian Todd Hefner

cc: Grant & Contract Administrator, APL-UW
Office of Sponsored Programs, UW
Naval Research Laboratory Code 5596
Defense Technical Information Center (electronic files with SF298)

Final Report

The Effects Of Sand Sediment Volume Heterogeneities On Sound Propagation And Scattering

Brian Todd Hefner
Applied Physics Laboratory, University of Washington, 1013 NE 40th Street, Seattle, WA 98105
phone: (206) 616-7558 fax: (206) 543-6785 email: hefner@apl.washington.edu

Award Number: N00014-10-1-0089
http://oa.apl.washington.edu

RESEARCH GOALS

The goal of the proposed research was to further develop and test models of volume scattering by utilizing the existing suite of instrumentation previously developed at APL-UW for the study of high-frequency acoustics. In order to perform the data/model comparisons, extensive environmental characterization was also to be performed in the pond and at-sea.

TECHNICAL APPROACH

FY10

APL-UW and NSWC-PCD are participating in an experiment in the NSWC test pond in the spring of FY10. Drs. Steven Kargl and Joseph Lopes are leading this effort. In order to perform the backscattering measurements utilizing the equipment to be deployed in the pond, a one-week extension will be added to this experiment. This extension will focus on backscattering measurements from a smoothed interface as was done in FY09 as well as from more complicated sediment manipulations including the addition of coarse grains, shell distributions, sediment layers, and interface roughness.
The environmental characterization in the pond during this experiment will include conductivity probe measurements using the In-situ Measurement of Porosity (IMP2) system, roughness measurements using the IMP2/LLS, sound speed and attenuation measurements using the Sediment Transmission and Measurement System (STMS1), and diver cores which will be collected for high-resolution CT scans for volume heterogeneity. All of these systems are scheduled for deployment during the Kargl/Lopes experiment and the work proposed here will leverage the existing effort.

Accomplishments: The one-week experiment took place in the NSWC test facility. High frequency backscatter and sediment propagation data was collected along with

environmental measurements of the sediment. These measurements are discussed in a proceedings paper submitted to the European Conference on Underwater Acoustics in 2010.

FY11

Following the experiments in FY10, a second set of experiments will be performed either in the NSWC pond or in laboratory facilities at APL-UW. The ability to conduct experiments in the pond will depend on whether funding is available to deploy the APL-UW rail system for continued SAS experiments. If this should not be possible, extensive scattering experiments will be conducted at APL-UW. In either case, these experiments will explore issues raised by the experiments in FY10.

Accomplishments: In January 2011, I was asked by ONR (Ben Reeder) to be co-chief scientist for the TREX13 experiment. A portion of my funding therefore went towards planning and preparation for the 2013 experiment. In the spring of 2011, an engineering test was conducted in the Gulf of Mexico at the future TREX13 site. This test was leveraged to collect environmental data using APL-UW assets with funds from this grant. This data was used to aid site selection and as input to preliminary acoustic modeling for the experiment. On June 1, 2011, the first reverberation workshop was held in Washington, DC. Analysis of the 2010 pond data continued, as did theory development. The results of this progress were presented in a proceedings paper submitted to the European Conference on Underwater Acoustics in 2012.

FY12

Field Experiment: While the pond experiments will be performed to utilize a controlled environment, the FY12 effort will focus on a more complicated, shallow-water environment similar to SAX99 and SAX04. This experiment will again use the bistatic array deployed with the APL-UW rail system in an attempt to resolve some of the outstanding questions that remain from SAX04. This effort will be performed in conjunction with a Reverberation Field Experiment (RFE) being proposed by Dr. Tang.

Accomplishments: In the spring of 2012, a pilot experiment for TREX13 was conducted in the Gulf of Mexico. During this experiment, backscattering data and environmental parameters were collected at the experiment site. This data and preliminary analysis was presented at the fall 2012 ASA meeting. This experiment also showed us that the In-Situ Measurement of Porosity (IMP2) system needed a substantial overhaul in preparation for TREX13. A portion of the grant was used to fund this successful refurbishment and the system was deployed extensively during TREX13. Planning continued for the 2013 experiment with workshops held in January and October 2012.

REPORT DOCUMENTATION PAGE

Form Approved
OMB No. 0704-0188

PLEASE DO NOT RETURN YOUR FORM TO THE ABOVE ADDRESS.

1. REPORT DATE *(DD-MM-YYYY)*	2. REPORT TYPE	3. DATES COVERED *(From - To)*
19 August 2013	Final Technical Report	01-Jan-2010 -- 30-June-2013

4. TITLE AND SUBTITLE

The effects of sand sediment volume heterogeneities on sound propagation and scattering

5a. CONTRACT NUMBER

5b. GRANT NUMBER

N00014-10-1-0089

5c. PROGRAM ELEMENT NUMBER

6. AUTHOR(S)

Brian Todd Hefner, University of Washington

5d. PROJECT NUMBER

5e. TASK NUMBER

5f. WORK UNIT NUMBER

7. PERFORMING ORGANIZATION NAME(S) AND ADDRESS(ES)

Applied Physics Laboratory
University of Washington
1014 NE 40th St.
Seattle, WA 98105

8. PERFORMING ORGANIZATION REPORT NUMBER

9. SPONSORING/MONITORING AGENCY NAME(S) AND ADDRESS(ES)

Dr. Robert Headrick, Code 322
Office of Naval Research
875 North Randolph Street
Arlington, VA 22203

10. SPONSOR/MONITOR'S ACRONYM(S)

ONR

11. SPONSOR/MONITOR'S REPORT NUMBER(S)

12. DISTRIBUTION/AVAILABILITY STATEMENT

Distribution Statement A: Approved for public release, distribution unlimited.

13. SUPPLEMENTARY NOTES

14. ABSTRACT

Despite their prevalence in shallow water environments, sand sediments remain poorly understood acoustic media, with one of the largest gaps in our understanding lying at the high (>100 kHz) frequencies. This lack of understanding has important consequences for many practical applications including the remote sensing of sediment properties.

The goal of the proposed research was to further develop and test models of volume scattering by utilizing the existing suite of instrumentation previously developed at APL- UW for the study of high-frequency acoustics. In order to perform the data/model comparisons, extensive environmental characterization was also to be performed in the pond and at-sea.1ln(1= h). The approach tow by the scintillation index, is exponential: ˙2(t) 12 exp(• • t)ln(1= h) + 1 + O(h=t2). Thi quantum signature of classical chaos.

h e.1ln(1= h). The approach toward equilibrium, as measured by the scintillation index, is exponential: ˙2(t) 12 exp(• • t)ln(1= h) + 1 + O(h=t2). This provides a quantum signature of classical chaos.

15. SUBJECT TERMS

volume scattering, high frequency, porosity fluctuations, reverberation

16. SECURITY CLASSIFICATION OF:			17. LIMITATION OF ABSTRACT	18. NUMBER OF PAGES	19a. NAME OF RESPONSIBLE PERSON
a. REPORT	b. ABSTRACT	c. THIS PAGE			Brian Todd Hefner
U	U	U	U		19b. TELEPHONE NUMBER *(Include area code)* (206) 616-7558

Reset

Enclosure 2

Attenuation in Sand Sediments Due to Scattering from Porosity Fluctuations.

Brian T. Hefner and Darrell R. Jackson

Applied Physics Laboratory,

University of Washington,

1013 NE 40th St,

Seattle,

WA 98105

(Dated: September 10, 2013)

Abstract

At high frequencies, the attenuation measured in sand sediments is larger then the predictions of Biot theory. To account for this discrepancy, perturbation theory is used to incorporate losses due to scattering by porosity variations into both Biot's poroelastic equations and the effective density fluid model. While previous results showed that fluctuations in the bulk frame modulus were insufficient to produce significant attenuation in a sand sediment, modest levels of fluctuations in the porosity produce significant scattering loss. By using the sediment parameters and the heterogeneity power spectrum measured during the Sediment Acoustics Experiment in 2004, the perturbation theory result shows good agreement with the sound speed and attenuation data without any free parameters.

PACS numbers: 43.30.Ma, 43.20.Gp, 43.20.Jr

I. INTRODUCTION

High-frequency sound propagation in fluid-saturated, unconsolidated granular media, including ocean sediments, exhibits attenuation greater than is predicted by Biot theory. When the wavelength is less than the grain diameter, the attenuation goes as f^4 and the dominant loss mechanism is likely scattering from the individual grains[1,2]. When the wavelength is longer than the mean grain diameter in the medium, the attenuation often exhibits a linear frequency dependence as opposed to the $f^{1/2}$ dependence predicted by Biot theory[3–5]. For sand sediments, models have been proposed which introduce additional loss mechanisms, such as squirt-flow[1,6] or friction, at the grain contacts and either use Biot Theory or an additional grain contact model to account for the low frequency attenuation[7].

Adding a loss mechanism at the grain contacts follows from observations made elsewhere in the granular physics community. Dry granular materials have frictional losses at the grain contacts and it is logical to assume that similar losses would be present in a fluid-saturated medium. The difficulty with this approach is that these models involve grain contact parameters that must be determined from empirical fits to the sound speed and attenuation data. In most cases, the required parameters do not even have a clear connection to any measurable geophysical parameter, such as the fluid viscosity or the grain bulk modulus, and are instead constants in a spring-dashpot model of the contact.

The model presented here also considers the importance of the granular nature of a sand sediment, but instead of positing loss mechanisms at the grain contacts, we consider losses due to the scattering of sound from variations in the sediment pore structure. This approach builds on theory developed previously to account for scattering from variations in the bulk frame modulus[8]. In that work, we applied perturbation theory to Biot's poroelastic equations and found that in an ocean sediment the frame moduli are too weak to produce significant scattering contributions to the attenuation. The degree to which variations in any sediment parameter will lead to scattering depends on how strongly those variations affect the local wavenumber in the medium. In Ref. 3, the authors examined how much the

sound speed and attenuation varied over the uncertainty ranges of the measured sediment parameters. While the limits of the frame bulk modulus uncertainties were roughly %40 of the mean value, neither the sound speed nor the attenuation showed any significant effect. Small changes in the porosity (%4), however, produced significant changes in the modeled sound speed. It seems likely then that the local wavenumber will vary greatly in a medium with variations in porosity thus producing significant scattering losses.

To determine the degree to which scattering from porosity variations contributes to the attenuation, we will apply perturbation theory to Biots poroelastic equations using the same approach used previously for moduli variations. Since the goal is to understand propagation in sand sediments, only weakly consolidated sediments will be considered, specifically sediments where $K_b, \mu_b \ll K_g$ where K_b, μ_b, and K_g are the frame bulk, frame shear, and grain moduli respectively. Previously it was found that porosity variations only weakly scatter energy into the Biot slow wave and the shear wave[9]. This is confirmed here for the scattering into the slow wave and the focus will be primarily on losses due to scattering into incoherent fast compressional waves.

This scattering is incorporated using perturbation theory in Section III for both the full Biot poroelastic equations and the effective density fluid model (EDFM). The resulting wave equations are solved first for the exponential correlation function in Section IV. While the exponential function provides insight into effects of the random medium on the sound propagation, it does not produce the linear attenuation observed in sand sediments. In order to fit the measured data, a correlation function is introduced in section V that has a corresponding power spectrum that can provide a broad range of spectral slopes. This correlation function is shown to fit the attenuation and sound speed measured in the Sediment Acoustics Experiment in 1999 and the parameters required to produce this fit and their implications for the statistics of the sediment are discussed in Section VII.

II. HETEROGENOUS BIOT POROELASTIC EQUATIONS

To examine the effect of porosity heterogeneities on sound propagation, we will apply perturbation theory to Biot's poroelastic equations. In Ref.8, these were given where both the frame moduli and the porosity were allowed to vary as a function of position. When the frame moduli are assumed to be constant, the equations have the same form,

$$\partial_i[(H-2\mu_b)\,\nabla\cdot\mathbf{u}-C\nabla\cdot\mathbf{w}]+ \tag{1}$$
$$\partial_j\left[\mu_b\left(\partial_i u_j+\partial_j u_i\right)\right]=-\omega^2\rho u_i+\omega^2\rho_f w_i$$

and

$$\partial_i\left[C\nabla\cdot\mathbf{u}-M\nabla\cdot\mathbf{w}\right]=-\omega^2\rho_f u_i+\omega^2\rho^* w_i, \tag{2}$$

where $\mathbf{u}$ is the displacement of the frame, $\mathbf{w}=\beta\left(\mathbf{u}-\mathbf{u_f}\right)$ is the relative displacement of the pore fluid to the frame, $\mathbf{u_f}$ is the displacement of the pore fluid, ρ_g is the sediment particle mass density, and

$$H=\frac{\left(K_g-K_b\right)^2}{D-K_b}+K_b+\frac{4\mu_b}{3}, \tag{3}$$

$$C=\frac{K_g\left(K_g-K_b\right)}{D-K_b}, \tag{4}$$

$$M=\frac{K_g^2}{D-K_b}, \tag{5}$$

$$D=K_g\left[1+\beta\left(\frac{K_g}{K_f}-1\right)\right], \tag{6}$$

$$\rho=\left(1-\beta\right)\rho_g+\beta\rho_f, \tag{7}$$

and

$$\rho^*=\frac{\alpha\rho_f}{\beta}+\frac{iF\eta}{\kappa\omega}, \tag{8}$$

where K_f is the bulk modulus of the pore fluid, α is the tortuosity, and the parameter F represents the deviation from Poiseuille flow as frequency increases. The expression for F is given and discussed in Ref.3.

As was done previously, these equations can be consolidated into a single, matrix equation as

$$\nabla\left[[\mathsf{K}]\,\nabla\cdot\mathbf{U}\right]-[\tilde{\mu}_0]\,\nabla\times\left(\nabla\times\mathbf{U}\right)+[\rho]\,\omega^2\mathbf{U}=0 \tag{9}$$

where

$$[\mathsf{K}] = \begin{bmatrix} H & -C \\ C & -M \end{bmatrix}, \tag{10}$$

$$[\boldsymbol{\rho}] = \begin{bmatrix} \rho & -\rho_f \\ \rho_f & -\rho^* \end{bmatrix}, \tag{11}$$

$$[\tilde{\boldsymbol{\mu}}] = \begin{bmatrix} \mu_b & 0 \\ 0 & 0 \end{bmatrix}, \tag{12}$$

and

$$\mathbf{U} = \begin{bmatrix} \mathbf{u} \\ \mathbf{w} \end{bmatrix}. \tag{13}$$

which for the homogeneous case, when $[\mathsf{K}] = [\mathsf{K}_0]$ and $[\boldsymbol{\rho}] = [\boldsymbol{\rho}_0]$ are constants, reduces to

$$\left([\mathsf{K}_0] - [\tilde{\boldsymbol{\mu}}_0]\right) \nabla \left(\nabla \cdot \mathbf{U}\right) + [\tilde{\boldsymbol{\mu}}_0] \, \nabla^2 \mathbf{U} + [\boldsymbol{\rho}_0] \, \omega^2 \mathbf{U} = 0. \tag{14}$$

This equation admits three solutions: fast and slow compressional waves and a shear wave.

For a typical sand sediment, the frame moduli are much smaller then the grain and fluid moduli and the medium only weakly supports the Biot slow wave and the shear wave. In the limit as $K_b = \mu_b = 0$, the medium can be described as a fluid with an effective compressibility,

$$\kappa = (1 - \beta) \, \kappa_g + \beta \kappa_w, \tag{15}$$

and an effective density,

$$\rho_{\text{eff}} = \frac{\rho \rho^* - \rho_w^2}{\rho^* + \rho - 2\rho_w}, \tag{16}$$

This description of a poroelastic medium is referred to as the effective density fluid model (EDFM)[10]. The equation of motion for the EDFM reduces to

$$\nabla \cdot \left(\frac{1}{\rho_{\text{eff}}} \nabla p \right) + \omega^2 \kappa p = 0, \tag{17}$$

where the effective pressure, p, is related to the effective displacement in the medium,

$$\mathbf{u}_{\text{eff}} = (1 - \beta) \, \mathbf{u} - \beta \mathbf{u}_f, \tag{18}$$

through

$$p = -\frac{1}{\kappa_{\text{eff}}} \nabla \cdot \mathbf{u}_{\text{eff}}. \tag{19}$$

In a homogeneous medium, the equation of motion simplifies to

$$\nabla^2 p + k_{\text{eff}}^2 p = 0 \tag{20}$$

and the wavenumber in this medium is

$$k_{\text{eff}} = \omega \sqrt{\rho_{\text{eff}} \kappa}. \tag{21}$$

In the following, we will consider perturbations to both Eq. (9) and Eq. (17).

III. PERTURBATION THEORY

To understand the role of the porosity fluctuations in sound propagation through the sediment, we will consider a poroelastic medium where the porosity varies with position,

$$\beta(\mathbf{r}) = \beta_0 + \delta\beta(\mathbf{r}). \tag{22}$$

We will also assume that a porous medium can be described by Biot's poroelastic equations and use perturbation theory to determine the effect of scattering on the fast compressional wave. In the specific case of a sand sediment, perturbation theory will also be applied to the effective density fluid model.

There are two approaches to solving for the mean wavenumber. The first converts the scattering equation into an integral equation for the Green's function for the inhomogeneous medium. This equation is solved iteratively to obtain the Dyson equation which is then truncated for a first order approximation. This approach was used by Rytov et al[11] for an inhomogeneous fluid medium and more recently by Muller and Gurevich[12] for an inhomogeneous poroelastic medium. In the latter case, only the losses due to mode conversion between the fast and slow compressional waves were considered in the low-frequency approximation.

In the approach taken here, perturbation theory is applied to the wave equation in an inhomogeneous medium and then solved iteratively for the mean field. This yields a series

solution which is truncated to yield the solution up to second order. The resulting equation is solved for plane wave propagation to find the effective wavenumber. This approach was developed by Karal and Keller[13] for the general case of scalar, elastic, or electromagnetic wave propagation in a random medium and later extended to poroelastic wave propagation[8]. While both of these approaches give the same results for the mean wavenumber in the medium, the solution to the Dyson equation also provides an approximation to the Green's function. Since our primary interest is to explore the effects of scattering on the dispersion and attenuation in medium, we will use the approach developed in Ref. 8.

A. Perturbation theory applied to Biot's equations

In Biot's poroelastic equations, both the moduli and density matrices are functions of the porosity. By assuming that the fluctuations are small, we can expand these matrices about the mean porosity,

$$[\mathsf{K}] = [\mathsf{K}_0] + [\mathsf{F}_{\mathsf{K}1}]\,\delta\beta + \frac{1}{2}\,[\mathsf{F}_{\mathsf{K}2}]\,\delta\beta^2 + \ldots \tag{23}$$

and

$$[\rho] = [\rho_0] + [\mathsf{F}_{\rho 1}]\,\delta\beta + \frac{1}{2}\,[\mathsf{F}_{\rho 2}]\,\delta\beta^2 + \ldots, \tag{24}$$

where

$$[\mathsf{F}_{\mathsf{K}n}] = \frac{\partial^n\,[\mathsf{K}_0]}{\partial\beta^n} \tag{25}$$

and

$$[\mathsf{F}_{\rho n}] = \frac{\partial^n\,[\rho_0]}{\partial\beta^n}. \tag{26}$$

This situation differs from the case of frame moduli variations which was explored in Ref. 8, where only the moduli matrix was affected. It was possible to take the divergence of Eq. (9) to find the wave equation,

$$\nabla^2\,[[\mathsf{K}]\,\nabla\cdot\mathbf{U}] + [\rho]\,\omega^2\nabla\cdot\mathbf{U} = 0. \tag{27}$$

Expressing the displacement in terms of potentials,

$$\mathbf{U} = \nabla\Phi + \nabla\times\mathbf{\Psi}, \tag{28}$$

the wave equation becomes

$$[\mathsf{K}]\,\nabla^2\Phi + [\rho]\,\omega^2\Phi = 0, \tag{29}$$

where

$$\Phi = \begin{bmatrix} \phi_u \\ \phi_w \end{bmatrix}. \tag{30}$$

This means that the moduli variations do not lead to mode conversion between the compressional and shear waves and a simplified version of the poroelastic Green's function can be used.

In the case of porosity variations, the wave equation cannot be reduced to Eq. (27) unless

$$\nabla\delta\beta \approx 0, \tag{31}$$

in which case $\nabla\,[\rho] = 0$. When Eq. (31) is not used, the full poroelastic Green's function is necessary and energy can be scattered into both the compressional and shear waves. This yields a much more complicated wave equation. For a sand sediment there is no appreciable difference in the attenuation when the approximation above is used[9]. Since we are interested in the attenuation of a sand sediment, we will proceed by assuming that the condition given by Eq. (31) is valid. This will be revisited in Appendix **??** where we give the full solution to the EDFM perturbation equation.

With this assumption, we can apply perturbation theory to the wave equation for the scalar potential, Eq. (29), which we will write as

$$\mathrm{L}\left([\mathsf{K}]\,,[\rho]\right)\Phi = 0. \tag{32}$$

Substitution of the expanded matrices produces

$$(\mathrm{L}_0 + \mathrm{L}_1 + \mathrm{L}_2 + \dots\,)\,\Phi = 0, \tag{33}$$

where $\mathrm{L}_0\Phi = 0$ is the homogeneous wave equation,

$$\mathrm{L}_1\Phi = [\mathsf{F}_{\mathsf{K}1}]\,\delta\beta\nabla^2\Phi + [\mathsf{F}_{\rho 1}]\,\delta\beta\omega^2\Phi, \tag{34}$$

and

$$\mathrm{L}_2\Phi = \frac{1}{2}\left(\left[\mathsf{F}_{\mathsf{K}2}\right]\delta\beta^2\nabla^2\Phi + \left[\mathsf{F}_{\rho 2}\right]\delta\beta^2\omega^2\Phi\right). \tag{35}$$

By assuming the propagating field is the sum of a scattered, incoherent component and a coherent component, the wave equation for the mean propagating field in the heterogeneous medium can be expressed to second order as,

$$\begin{aligned}
&\mathrm{L}_0\left\langle\Phi\left(\mathbf{r}\right)\right\rangle \\
&+\left\langle \mathrm{L}_1\left(\mathbf{r}\right)\int\left[\mathsf{G}\left(\mathbf{r},\mathbf{r}'\right)\right]\mathrm{L}_1\left(\mathbf{r}'\right)\left\langle\Phi\left(\mathbf{r}'\right)\right\rangle d^3\mathbf{r}'\right\rangle \\
&+\left\langle \mathrm{L}_2\left(\mathbf{r}\right)\left\langle\Phi\left(\mathbf{r}\right)\right\rangle\right\rangle = 0,
\end{aligned} \tag{36}$$

where

$$\left[\mathsf{G}\left(\mathbf{r},\mathbf{r}'\right)\right] = \sum_{n=1}^{2}\left[\mathsf{G}_n\right]k_n^2 g_n\left(\mathbf{r},\mathbf{r}'\right) \tag{37}$$

is the Biot Green's function for a compressional point source, $n = 1$ and 2 correspond to the fast and slow compressional waves, $[\mathsf{G}_n]$ is given in Eq. (A4) and (A5) of Ref. 8, and

$$g_n\left(\mathbf{r},\mathbf{r}'\right) = \frac{\mathrm{e}^{ik_n|\mathbf{r}-\mathbf{r}'|}}{4\pi\left|\mathbf{r}-\mathbf{r}'\right|} \tag{38}$$

is the scalar Green's function. This expression was derived for a poroelastic medium for the full vector displacement in Ref. 8 and it is straightforward to show that Eq. (36) is the appropriate expression for the coherent scalar potential.

Using Eq. (34), the second term in Eq. (36) becomes

$$\begin{aligned}
&\left\langle \mathrm{L}_1\left(\mathbf{r}\right)\int\left[\mathsf{G}\left(\mathbf{r},\mathbf{r}'\right)\right]\mathrm{L}_1\left(\mathbf{r}'\right)\left\langle\Phi\left(\mathbf{r}'\right)\right\rangle d^3\mathbf{r}'\right\rangle \\
&= \left[\mathsf{F}_{\mathsf{K}1}\right]\sum_{n=1}^{2}\left[\mathsf{G}_n\right]k_n^2\left[\mathsf{F}_{\mathsf{K}1}\right]\int\nabla^2 g_n(R)C(R)\nabla'^2\left\langle\Phi\left(\mathbf{r}'\right)\right\rangle d^3\mathbf{r}' \\
&+\left[\mathsf{F}_{\mathsf{K}1}\right]\sum_{n=1}^{2}\left[\mathsf{G}_n\right]k_n^2\left[\mathsf{F}_{\rho 1}\right]\omega^2\int\nabla^2 g_n(R)C(R)\left\langle\Phi\left(\mathbf{r}'\right)\right\rangle d^3\mathbf{r}' \\
&+\left[\mathsf{F}_{\rho 1}\right]\sum_{n=1}^{2}\left[\mathsf{G}_n\right]k_n^2\left[\mathsf{F}_{\mathsf{K}1}\right]\omega^2\int g_n(R)C(R)\nabla'^2\left\langle\Phi\left(\mathbf{r}'\right)\right\rangle d^3\mathbf{r}' \\
&+\left[\mathsf{F}_{\rho 1}\right]\sum_{n=1}^{2}\left[\mathsf{G}_n\right]k_n^2\left[\mathsf{F}_{\rho 1}\right]\omega^4\int g_n(R)C(R)\left\langle\Phi\left(\mathbf{r}'\right)\right\rangle d^3\mathbf{r}',
\end{aligned} \tag{39}$$

where $C(\mathbf{r},\mathbf{r}') = \langle \delta\beta(\mathbf{r})\,\delta\beta(\mathbf{r}')\rangle$ since the mean is taken only over the product of the porosity variations. If we assume that the variations in the porosity are statistically homogeneous (spatially stationary) and isotropic, then the covariance should depend only on the distance $R = |\mathbf{r}-\mathbf{r}'|$ and $C(\mathbf{r},\mathbf{r}') = C(R)$.

Using the inhomogeneous wave equation for the scalar Green's function,

$$\nabla^2 g_n(R) = -k_n^2 g_n(R) - \delta(R), \tag{40}$$

and assuming a plane wave solution for the mean potential,

$$\langle \Phi(\mathbf{r})\rangle = A\mathrm{e}^{i\mathbf{k}\cdot\mathbf{r}}, \tag{41}$$

the expression in Eq. (39) becomes

$$\begin{aligned}
&\left\langle \mathrm{L}_1(\mathbf{r}) \int [\mathsf{G}(\mathbf{r},\mathbf{r}')]\,\mathrm{L}_1(\mathbf{r}')\,\langle\Phi(\mathbf{r}')\rangle\, d^3\mathbf{r}' \right\rangle \\
&= \Bigg[[\mathsf{F}_{\mathsf{K}1}] \sum_{n=1}^{2} [\mathsf{G}_n]\, k_n^4 \left([\mathsf{F}_{\mathsf{K}1}]\, k^2 - [\mathsf{F}_{\rho 1}]\,\omega^2 \right) \\
&- [\mathsf{F}_{\rho 1}] \sum_{n=1}^{2} [\mathsf{G}_n]\, k_n^2 \left([\mathsf{F}_{\mathsf{K}1}]\,\omega^2 k^2 + [\mathsf{F}_{\rho 1}]\,\omega^4 \right) \Bigg] I_n \\
&+ [\mathsf{F}_{\mathsf{K}1}] \sum_{n=1}^{2} [\mathsf{G}_n]\, k_n^2 \left([\mathsf{F}_{\mathsf{K}1}]\, k^2 - [\mathsf{F}_{\rho 1}]\,\omega^2 \right) \sigma^2 \langle\Phi\rangle,
\end{aligned} \tag{42}$$

where $\sigma^2 = C(0)$ is the variance of the porosity variations and

$$I_n = \int g_n(R)\, C(R)\, \langle \Phi(\mathbf{r}')\rangle\, d^3\mathbf{r}'. \tag{43}$$

The third term in Eq. (36) can be written using Eq. (35) as

$$\langle \mathrm{L}_2(\mathbf{r})\,\langle\Phi(\mathbf{r})\rangle\rangle = \frac{1}{2}\left([\mathsf{F}_{\mathsf{K}2}]\, k^2 + [\mathsf{F}_{\rho 2}]\,\omega^2 \right) \sigma^2 \langle\Phi\rangle, \tag{44}$$

and the wave equation for the mean scalar field can be written as

$$-k^2 [\mathsf{K}_{\mathsf{eff}}]\,\langle\Phi\rangle + \omega^2 [\rho_{\mathsf{eff}}]\,\langle\Phi\rangle = 0, \tag{45}$$

where the effective modulus and porosity matrices are

$$\begin{aligned}[\mathsf{K_{eff}}] &= [\mathsf{K_0}] \\ &- \sum_{n=1}^{2} \left([\mathsf{F_{K1}}]\, k_n^2 - [\mathsf{F}_{\rho 1}]\, \omega^2 \right) [\mathsf{G}_n]\, k_n^2\, [\mathsf{F_{K1}}]\, I_n \\ &- \left([\mathsf{F_{K1}}]\, [\mathsf{K_0}]^{-1}\, [\mathsf{F_{K1}}] - \frac{1}{2}\, [\mathsf{F_{K2}}] \right) \sigma^2 \end{aligned} \tag{46}$$

and

$$\begin{aligned}[\rho_{\mathsf{eff}}] &= [\rho_0] \\ &- \sum_{n=1}^{2} \left([\mathsf{F_{K1}}]\, k_n^2 - [\mathsf{F}_{\rho 1}]\, \omega^2 \right) [\mathsf{G}_n]\, k_n^2\, [\mathsf{F}_{\rho 1}]\, I_n \\ &- \left([\mathsf{F_{K1}}]\, [\mathsf{K_0}]^{-1}\, [\mathsf{F}_{\rho 1}] - \frac{1}{2}\, [\mathsf{F}_{\rho 2}] \right) \sigma^2. \end{aligned} \tag{47}$$

We have also used the relationship

$$\sum_{n=1}^{2} [\mathsf{G}_n]\, k_n^2 = [\mathsf{K_0}]^{-1}\,. \tag{48}$$

The integral in $[\mathsf{K_{eff}}]$ and $[\rho_{\mathsf{eff}}]$ given by Eq. (43) can be partially solved by separating it into its radial and surface components,

$$I_n = \int g_n\left(R\right) C\left(R\right) \int e^{-i\mathbf{k}\cdot\mathbf{R}} dS dR, \tag{49}$$

and the integration with respect to dS can be performed,

$$\int e^{-i\mathbf{k}\cdot\mathbf{R}} dS = \frac{4\pi R}{k} \sin kR. \tag{50}$$

Substituting this result back into Eq. (49) and substituting the expression in Eq. (38) for the scalar green's function, $g_n\left(R\right)$, the final integral is

$$I_n = \frac{1}{k} \int_0^{\infty} \mathrm{e}^{ik_n R} C\left(R\right) \sin\left(kR\right) dR. \tag{51}$$

With this expression for the integral, the solution to Eq. (45)-(47) yields the wave number for the mean coherent fast compressional wave propagating in an inhomogeneous poroelastic medium.

B. Perturbation theory applied to EDFM

For propagation in a random medium described by the EDFM, we expand the effective compressibility and density as Taylor series about $\delta\beta = 0$,

$$\rho_{eff} = \rho_0 + F_{\rho 1}\delta\beta + \frac{1}{2}F_{\rho 2} \tag{52}$$

and

$$\kappa_{eff} = \kappa_0 + F_{\kappa 1}\delta\beta, \tag{53}$$

where

$$F_{\rho n} = \frac{\partial^n \rho_0}{\partial \beta^n} \tag{54}$$

and

$$F_{\kappa n} = \frac{\partial^n \kappa_0}{\partial \beta^n}. \tag{55}$$

Note that $F_{\kappa n} = 0$ for $n > 1$.

We are now looking for the perturbation solution to the heterogeneous wave equation,

$$\left(L_0 + L_1 + L_2\right) p = 0, \tag{56}$$

where $L_0 p = 0$ is the homogenous wave equation,

$$L_1 = k_0^2 \left(F_{\rho 1} + F_{\kappa 1}\right) \delta\beta \tag{57}$$

and

$$L_2 = k_0^2 \left(F_{\rho 1} F_{\kappa 1} + \frac{1}{2}F_{\rho 2}\right) \delta\beta^2. \tag{58}$$

Using the scalar wave equation for the mean pressure given in Eq. (14) in Ref. 13, we can follow a similar procedure to that used in the derivation of the Biot theory result. Since for the EDFM we are dealing with only a single scalar field and not the vector of fields in Eq. (30), we can take the further step of solving for the effective wavenumber,

$$k^2 = k_0^2 \left(1 + F_2 \sigma^2\right) + F_1^2 k_0^4 I_0, \tag{59}$$

where

$$I_0 = \frac{1}{k}\int_0^\infty \mathrm{e}^{ik_0R} C\left(R\right)\sin\left(kR\right)dR, \tag{60}$$

$F_1 = F_{\rho 1} + F_{\kappa 1}$, and $F_2 = F_{\rho 1}F_{\kappa 1} + \frac{1}{2}F_{\rho 2}$.

For propagation through a random fluid medium, Rytov et al derived an approximation for the mean Green's function (Eq. (4.46) in Ref. 11). This expression contains an integral, the integrand of which yields a wavenumber equation that is identical to Eq. (59) to first order,

$$k^2 = k_0^2 + \frac{k_0^4}{k}\int_0^\infty \mathrm{e}^{ik_0R}\Psi\left(R\right)\sin\left(kR\right)dR, \tag{61}$$

where $\Psi\left(R\right) = F_1^2 C\left(R\right)$. The discussion of the solution to this equation given in Rytov et al and elsewhere will inform our examination of the solution for a poroelastic medium.

Before examining solutions to the perturbation wave equations, we will examine the assumption $\nabla\delta\beta \approx 0$ and consider under what circumstances this approximation is valid. For a fluid medium, we can relate the attenuation to the total scattering cross-section[14,15],

$$2\mathrm{Im}\left[k - k_0\right] = \sigma_{tv} = \int_{4\pi}\sigma_v d\omega, \tag{62}$$

where the differential cross-section for volume scattering due to heterogeneities in the porosity is

$$\sigma_v = \frac{\pi}{2}\left(F_{\kappa 1}k_0^2 + F_{\beta 1}\left(\mathbf{k}_i\cdot\mathbf{k}_s\right)\right)^2 W\left(k_d\right), \tag{63}$$

where $k_d = 2\mathrm{Re}\left[k_0\right]\sin\left(\theta/2\right)$ is the Bragg wavenumber. The compressibility fluctuations produce monopole scattering while the $\nabla\delta\beta$ term manifests in dipole scattering. As we will see in the next section, for an exponential correlation function, the power spectral density $W\left(k_d\right)$ has the form given by Eq. (65). When $\left(k_0L\right)^2 \gg 1$, the differential cross-section peaks in the forward-scattering direction ($\theta = 0$) and the dipole term becomes $\mathbf{k}_i\cdot\mathbf{k}_s = k_0^2$. This is equivalent to assuming $\nabla\delta\beta \approx 0$. Thus the assumption is therefore valid when $\left(k_0L\right)^2 \gg 1$. For all of the cases examined in the following, this condition is satisfied.

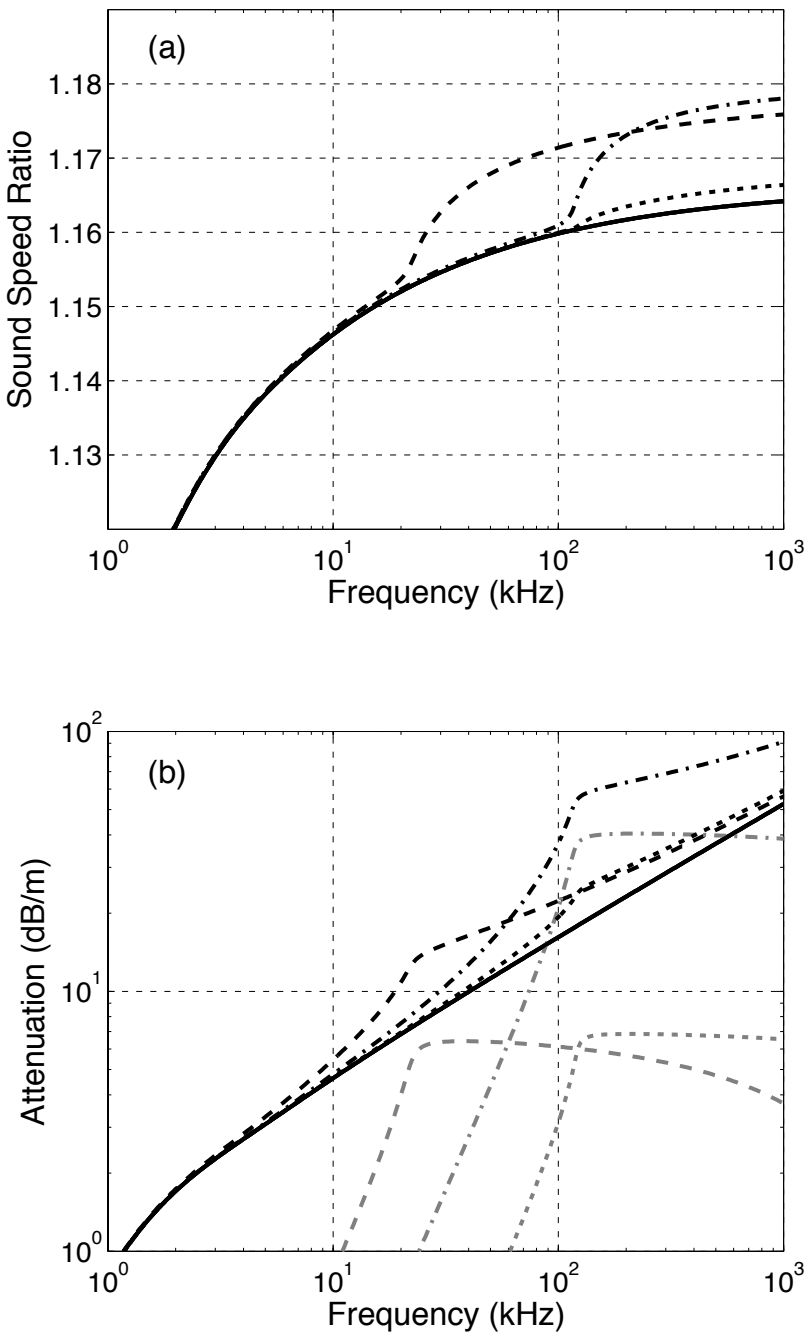

FIG. 1. Examples of the (a) sound speed ratio and (b) attenuation for the SAX04 sediment with porosity heterogeneities modeled using perturbation theory. The statistics of the heterogeneities are described by exponential correlation functions with (dashed line) $L = 0.6$ m and $\sigma = 0.042\beta$, (dashed-dotted line) $L = 0.1$ m and $\sigma = 0.05\beta$, and (dotted line) $L = 0.6$ m and $\sigma = 0.008\beta$. Also shown is the sound speed ratio and attenuation for the unperturbed medium (solid line). In (b) the differences between the perturbed and unperturbed attenuations are shown as the gray lines.

IV. EXPONENTIAL CORRELATION FUNCTION

In order to find a wavenumber solution to either Eq. (45) or (59), the integral given in Eq. (51) must be solved for a given correlation function. We will begin by considering the well-known exponential correlation function,

$$C_{exp}(R) = \sigma^2 e^{-\frac{R}{L}}, \tag{64}$$

where L is the correlation radius. This function has the corresponding power spectrum,

$$W(k) = \frac{\sigma^2}{\pi^2} \frac{L^3}{\left(1 + k^2 L^2\right)^2}, \tag{65}$$

that has a constant value for $kL \ll 1$ and goes as k^{-4} for $kL \gg 1$.

With this correlation function, the integrals in Eq. (51) and (60) have exact solutions:

$$I_n = \frac{\sigma^2 L^2}{\left(1 - ik_n L\right)^2 + k^2 L^2} \tag{66}$$

for Biot theory and

$$I_0 = I_{\exp} = \frac{\sigma^2 L^2}{\left(1 - ik_0 L\right)^2 + k^2 L^2} \tag{67}$$

for the EDFM. Since the integrals in Eq. (66) are themselves a function of the wavenumber, the Biot theory wave equation must be solved using a root-finding algorithm. This is not the case for EDFM where the equation can be written as a quadratic.

Taking the limit $L \to 0$ produces a medium where the variations are almost entirely uncorrelated. In this case, the integrals in Eq. (66) and Eq. (67) both go to zero. The effective modulus and porosity matrices then reduce to

$$\begin{aligned}[\mathsf{K}_{\mathsf{eff}}] &= [\mathsf{K}_0] \\ &\quad - \left([\mathsf{F}_{\mathsf{K1}}] [\mathsf{K}_0]^{-1} [\mathsf{F}_{\mathsf{K1}}] - \frac{1}{2} [\mathsf{F}_{\mathsf{K2}}] \right) \sigma^2 \end{aligned} \tag{68}$$

and

$$\begin{aligned}[\rho_{\mathsf{eff}}] &= [\rho_0] \\ &\quad - \left([\mathsf{F}_{\mathsf{K1}}] [\mathsf{K}_0]^{-1} [\mathsf{F}_{\rho 1}] - \frac{1}{2} [\mathsf{F}_{\rho 2}] \right) \sigma^2. \end{aligned} \tag{69}$$

In Appendix B of Ref. 8, we showed that in the case of frame modulus variations, the expression for $[K_{eff}]$ reduces to the effective response of a random poroelastic medium under static compression. The elastic response was dominated by the weaker elements and this "softening" had the effect of lowering the sound speed across all frequencies.

A similar analysis can be performed here to show that the effective moduli given above can be found by expanding

$$[K_{eff}]^{-1}[\rho_{eff}] = \left\langle [K(\mathbf{r})]^{-1}[\rho(\mathbf{r})] \right\rangle \tag{70}$$

about $\beta(\mathbf{r}) = \beta_0$. The moduli are dominated by the weaker and less dense regions in the medium with the density variations dominating the response. The net effect is to increase the sound speed. For the values of the variance considered here, this increase is slight and plays no significant role in any subsequent data/model comparisons.

Figure 1 shows the sound speed ratio and attenuation calculated using the Biot theory perturbation wave equation for several values of σ^2 and L using the sediment parameters given in Table I. Below a transition frequency, f_e, the sound speeds approximately follow the unperturbed sound speed while the attenuation contribution due to scattering increases as f^2. At f_e, the sound speed increases abruptly, while excess attenuation becomes constant. This transition frequency can be related to the correlation radius and variance according to

$$\frac{1}{4}|k_e|^2 L^2 \frac{\sigma^2}{\beta_0^2} \approx 1, \tag{71}$$

where k_e is the unperturbed fast compressional wave number corresponding to the transition frequency, while $\alpha \propto \sqrt{L\sigma}$ at the transition.

When perturbation theory was used previously to account for scattering losses in a medium with variations in the frame modulus, the size of the variations had to be extremely large ($\sigma_{bb} > 75\%$) to produce even a minor increase in attenuation. As shown in Fig. 1, small variations in the porosity ($\sigma < 5\%$) can produce a significant increase in the attenuation.

For the EDFM, the wavenumber equation can be solved analytically for the effective wavenumber when the exponential correlation function is used. The wavenumber equation can be written as a quadratic in k^2 with the solutions

$$k^2 = \left(k_e^2\Omega - \frac{\Lambda^2}{2L^2}\right)\left(1 \pm \sqrt{1 + 4k_e^2L^2\Theta}\right), \tag{72}$$

where

$$\Theta = \frac{\Omega\Lambda^2 + F_1^2\sigma^2k_e^2L^2}{\left(\Lambda^2 - \Omega k_e^2L^2\right)^2}, \tag{73}$$

$$\Lambda = (1 - ik_eL), \tag{74}$$

and

$$\Omega = \left(1 + F_2\sigma^2\right). \tag{75}$$

The root corresponding to the plus sign in Eq. (72) reduces to $k^2 = k_e^2\left(1 + F_2\sigma^2\right)$ as $\omega \to 0$ and produces the curve shown in Fig. 2.

As discussed in Section III, this solution reduces to the solution given by Rytov when $k_e = k_f$ and $F_2 = 0$. The roots of the wavenumber equation for that case are discussed extensively by Calvet and Margerin[16]. For the fluid case, they show that at low frequencies the sound speeds are nearly equal but diverge at high frequencies. The attenuation of the roots are nearly equal at high frequencies with one root that goes to zero as $\omega \to 0$ while the other root approaches a constant value of $\alpha = L^{-1}$. The solutions in Eq. (72) for the EDFM wavenumber equation behave similarly as do the solutions for the Biot perturbation wave equation. In both cases, we have chosen to focus on the root which most closely matches the unperturbed solution at low frequencies.

The effective density fluid model was developed as a simpler alternative to the full Biot theory when the frame moduli were much smaller then the grain and fluid moduli[10]. For the SAX99 data, for example, the EDFM was able to fit the measured data with the same accuracy as Biot theory[3]. Likewise in Fig. 2 the perturbation solution using EDFM approximates the Biot solution for the attenuation and with a minor deviation for the sound speed at high frequencies. For this choice of parameters, the error using EDFM at $f = 1$ MHz is 0.3% with comparable errors for other choices of parameters. Since for a sand sediment, the EDFM does not require that we solve a matrix equation and approximates

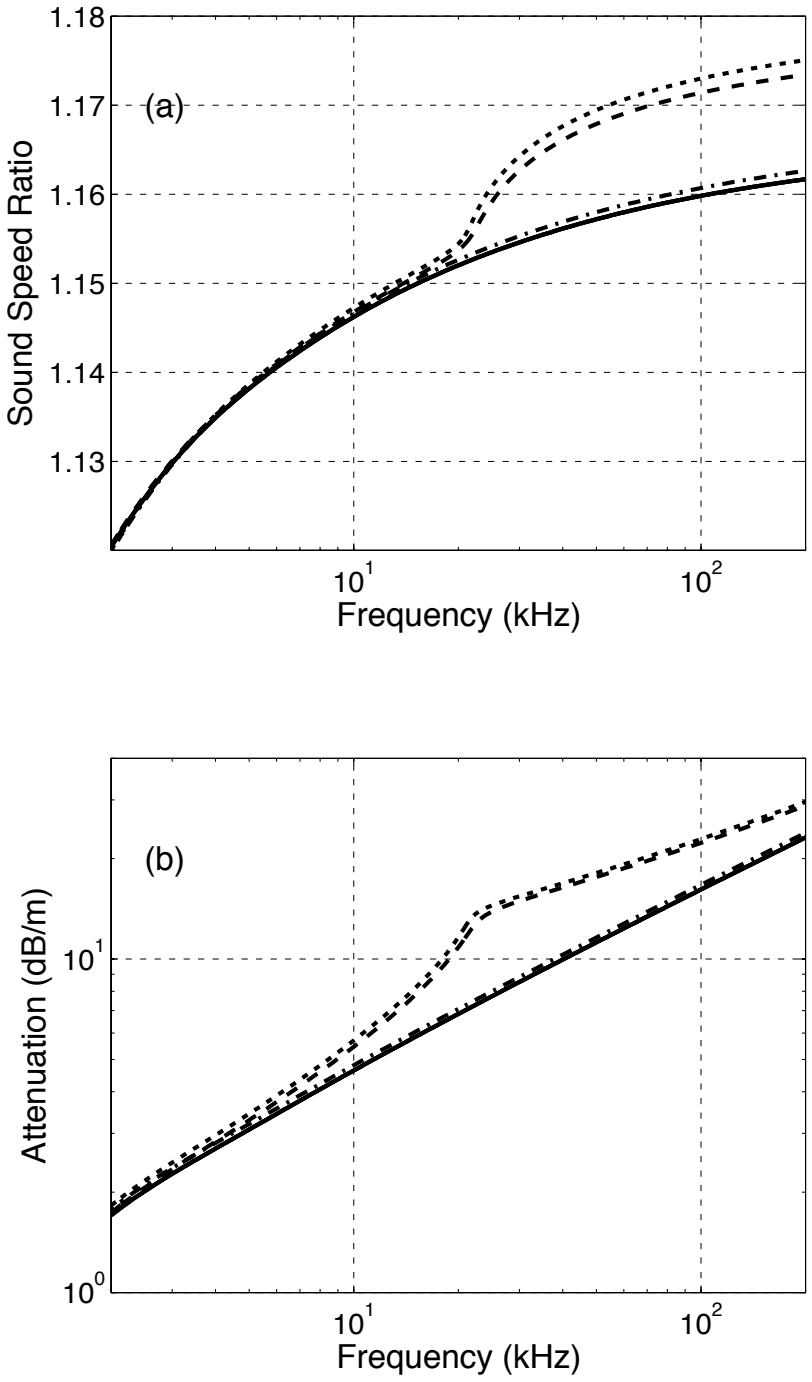

FIG. 2. Comparison of the (a) sound speed ratio and (b) attenuation for a heterogenous poroelastic medium modeled using perturbation theory applied to Biot Theory (dashed line) and the EDFM (dotted line). Also shown are the unperturbed sound speed and attenuation for Biot Theory (solid line) and the EDFM (dashed-dotted line).

the Biot theory solution, we will focus on the EDFM perturbation equation in the subsequent sections.

While an analytic solution to the perturbation equation can be found when using the exponential correlation function, the resulting sound speed and attenuation does not match the values measured in-situ or in the laboratory. The attenution due to scattering shown in Fig. 1 combines with the intrisic attenuation to produce a region that transitions from $\alpha \propto \sqrt{f}$ to $\alpha \propto f^2$ before returning to the intrinsic result. During this transition, there is a region in which the attenuation has a linear frequency dependence but it is confined to a very narrow band that would not fit the measured values. For scattering from heterogeneities to be a viable loss mechanism, a different statistical description of the medium is required. Ideally this description would come from measurements of the sediment structure, but for the following we will attempt to find a correlation function or spectral strength that can fit the data.

V. SUMMED EXPONENTIAL CORRELATION

At this point it would be logical to examine other common correlation functions or power spectra such as the von Karman power spectrum. For these more general spectra, the integral in the EDFM wave equation does not have a simple analytical solution. Solutions to the wavenumber equation would require that first the integral and then the wave equation be solved numerically.

To avoid this complication, we will consider instead a generalization of the exponential correlation function,

$$C_m(R) = A_m \int_{L_0}^{L_1} L^m e^{-\frac{R}{L}} dL, \tag{76}$$

where

$$A_m = \frac{\sigma^2}{L_1^{m+1} - L_0^{m+1}} \tag{77}$$

is chosen such that $C_m(0) = \sigma^2$. The integral in Eq. (60) now becomes

$$I_m = A_m \int_{L_0}^{L_1} \frac{L^{m+2}}{(1 - ik_0 L)^2 + k^2 L^2} dL. \tag{78}$$

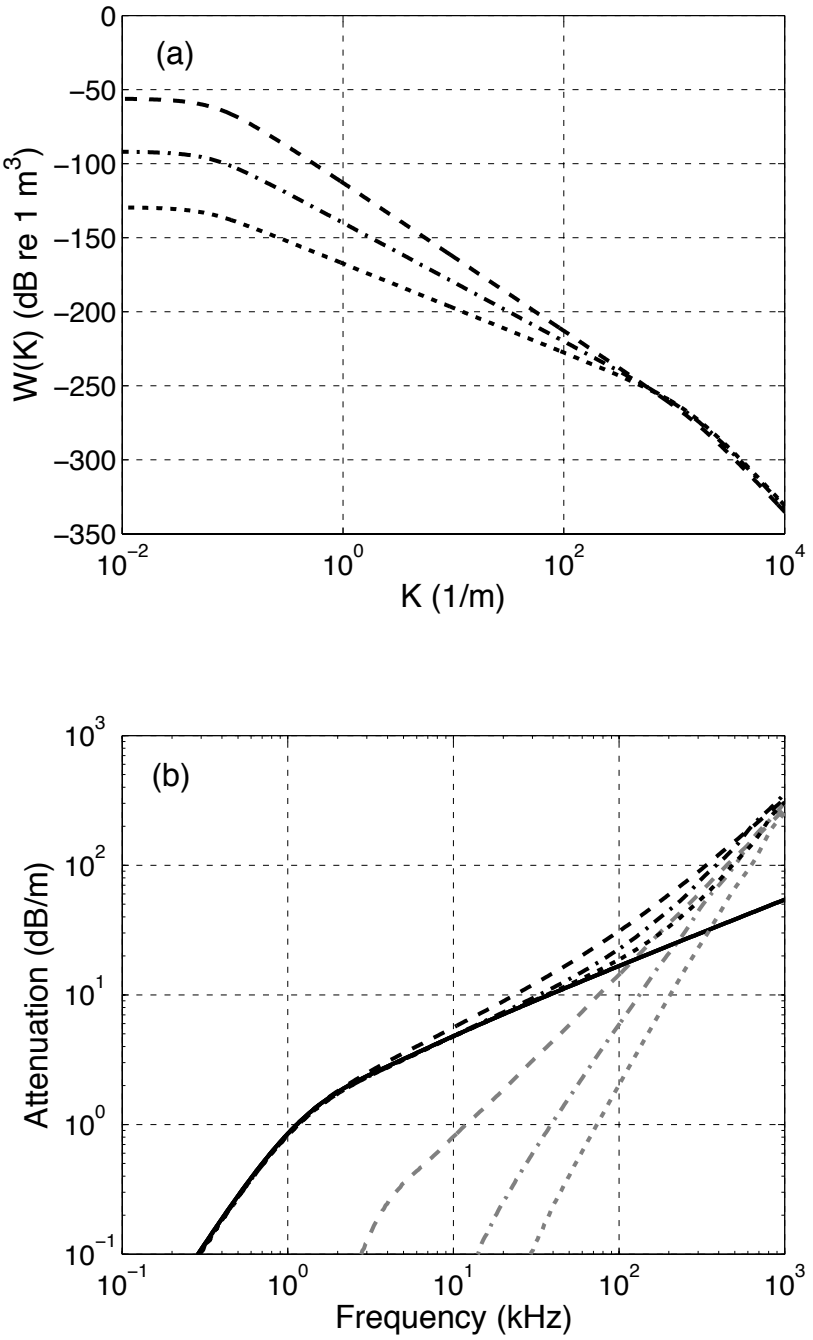

FIG. 3. (a) Power spectra calculated using Eq. (79) for $m = -1.5$ (dashed line), $m = -2.0$ (dasd-dot line), and $m = -2.5$ (dotted line) with $L_0 = 1$ mm, $L_1 = 1$ m, and $\sigma = 0.15\beta$. (b) Attenuation for sand sediment with porosity variations described by the power spectra given in (a) and the sediment properties given in Table I.

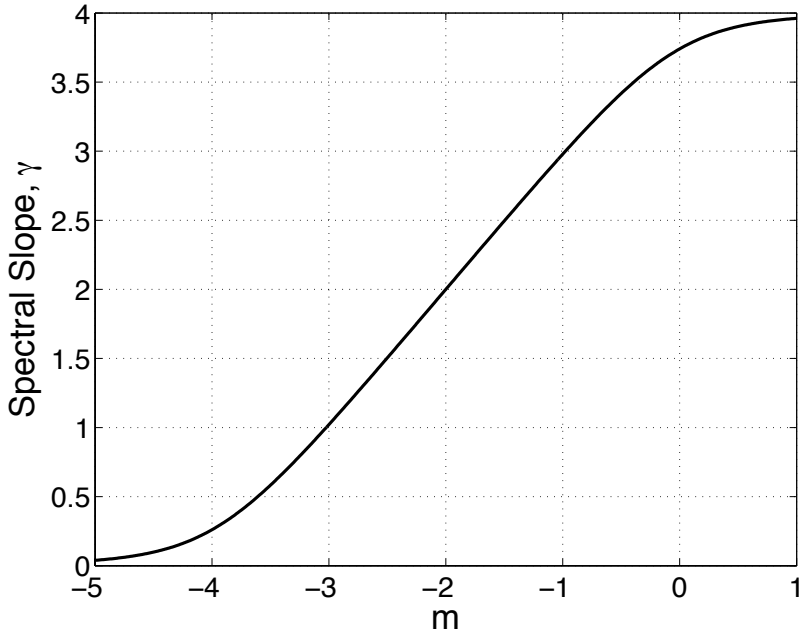

FIG. 4. Spectral slope, γ, as a function of m for the power spectrum given by Eq. (79) when $L_0 \ll k \ll L_1$.

The integration is now performed over a finite interval with a non-oscillating integrand. As will be shown below, it is straightforward to approximate this integral as a series.

To understand this choice of correlation function, consider the corresponding power spectrum,

$$W_m(k) = A_m \frac{m+1}{\pi^2} \int_{L_0}^{L_1} \frac{L^{m+3}}{\left(1+(kL)^2\right)^2} dL. \tag{79}$$

In the limit $k \ll L_0^{-1}, L_1^{-1}$, the power spectrum becomes

$$W_m(k) = \frac{\sigma^2}{\pi^2} \frac{m+1}{m+2} \frac{L_1^{m+4} - L_0^{m+4}}{L_1^{m+1} - L_0^{m+1}}, \tag{80}$$

while in the limit of $k \gg L_0^{-1}, L_1^{-1}$, the power spectrum is

$$W_m(k) = \frac{\sigma^2}{\pi^2} \frac{m+1}{m} \frac{L_1^m - L_0^m}{L_1^{m+1} - L_0^{m+1}} \frac{1}{k^4}. \tag{81}$$

The asymptotics of this spectrum reflect those of the exponential correlation function in the integrand. For values of the wavenumber such that $L_0^{-1} \ll k \ll L_1^{-1}$, the power spectrum

has a constant slope, γ, where $-4 < \gamma < 0$ (Fig. 3(a)). This dependence of the spectral slope on m is shown in Fig. 4 where the spectral slope can be well approximated by $\gamma = m + 3$.

To appreciate the utility of the power spectrum given in Eq. (79), we will compare it to the von Kàrmàn spectrum,

$$W_\nu(k) = \frac{L^3 \Gamma\left(\nu + \frac{3}{2}\right)}{\pi^{3/2} \Gamma(\nu) \left(1 + k^2 L^2\right)^{\frac{\gamma_3}{2}}}, \tag{82}$$

where $0 < \nu \leq 1$ and $\gamma_3 = 2\nu + 3$. When $\nu = 1/2$, this power spectrum reduces to that of the exponential correlation function with a spectrum proportional to k^{-4}. As $\nu \to 0$, the spectrum approaches k^{-3}. However, any spectrum that goes as k^γ with $\gamma > -3$ as $k \to \infty$ is unphysical since $\sigma^2 = \int_{-\infty}^{\infty} W(k)\, dk = \infty$.

An examination of Fig. 4 shows that this new spectrum can approximate the von Kàrmàn spectrum for $0 < \nu \leq 1/2$ over an arbitrary range of wavenumbers by choosing m such that $-1 < m \leq 1$. This greatly simplifies the evaluation of Eq. (60) for the von Kàrmàn correlation function. It is also possible to determine solutions to the perturbation wave equation when the fluctation power spectral slope exceeds $\gamma = -3$. The power spectrum given by Eq. (79) can produce a spectral slope that exceeds this limit over an arbitrary range of wavenumbers since $W(k \to \infty) \propto k^{-4}$. As we will see, this becomes important to produce a linear attenuation.

To find solutions to the EDFM perturbation wave equation, the integral given by Eq. (78) must be evaluated. The approach taken here is to approximate the correlation function, C_m, as a series. Using a linear spacing in L, the correlation function becomes

$$C_{m1}(R) = \frac{\sigma^2}{\sum_{n=0}^{N} L_n^m} \sum_{n=0}^{N} L_n^m e^{-\frac{R}{L_n}} \tag{83}$$

where $L_n = L_0 + n\Delta L$. An alternative way to approximate the integral is to choose the values of L_n such that they are logarithmically distributed. In this case,

$$C_{m2}(R) = \frac{\sigma^2}{\sum_{n=0}^{N} L_n^{m+1}} \sum_{n=0}^{N} L_n^{m+1} e^{-\frac{R}{L_n}}, \tag{84}$$

where $L_n = L_0 10^{n\Delta}$ and Δ determines the size of the logarithmic spacing. This approximation of the correlation function converges faster than the linear series since we are calculating

the sound speed and attenuation for frequencies that span several decades.

Using the series approximation given by Eq. (84), the integral in Eq. (60) becomes

$$I_0 = \frac{\sigma^2}{\sum_{n=0}^{N} L_n^{m+1}} \sum_{n=0}^{N} L_n^{m+1} I_{\exp}\left(L_n\right). \tag{85}$$

where $I_{\exp}$ is given in Eq. (67). The wave equation, Eq. (59), can now be solved numerically to determine the effective wavenumbers. The attenuation for media with porosity fluctuations described by the power spectra shown in Fig. 1(a) are shown in Fig. 1(b).

The scattering contributions to the attenuation are again determined by subtracting the unperturbed attenuation from the perturbation theory result. For the examples shown, these scattering contributions each have a power-law frequency dependence which varies from $f^{1.3}$ for $m = -1.5$ to $f^{2.2}$ for $m = -2.5$. The frequency dependence across m were calculated for the SAX04 sediment parameters and the powers are shown in Fig. 5. While these slopes are steeper than the linear frequency dependence shown in the data, the total attenuation is the sum of the intrinsic and scattering attenuations which produces a slope that transitions from $f^{1/5}$ to that of the scattering contribution.

In Fig. 5 the slope of the scattering contribution varies from 0.5 with $m \approx -0.5$ to 2.6 at $m = -5$. This lower value corresponds to the slope of the intrinsic attenuation and for this value of m the power spectrum approximates the von Kàrmàn spectrum with $\nu \approx 0.2$. At this m, the total attenuation goes as $f^{1/2}$, well below the linear attenuation. For $m < -2.2$, the power law exponent is larger then the value found for the exponential correlation function. With the correlation function given by Eq. (76) or the summation approximation given by Eq. (84), it is possible to model the frequency dependence of the attenuation for a broad range of exponents, beyond that which is accessible using the von Kàrmàn or exponential correlation functions.

VI. MODELING THE SAX04 DATA

Application of the perturbation wave equation, either the full Biot Theory or EDFM version, requires knowledge of the statistics of the heterogeneities in the sediment. In the

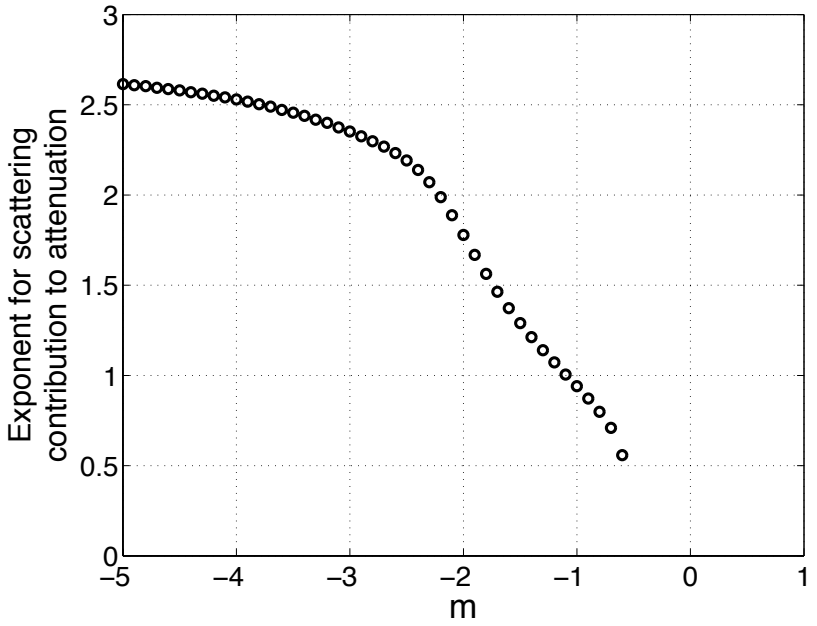

FIG. 5. Exponent for the scattering contribution to the attenuation determined by solving the EDFM perturbation wave equation with $L_0 = 1$ mm, $L_1 = 1$ m, and $\sigma = 0.20\beta$. The scattering contribution is the difference between the attenuation in a heterogenous medium and the attenuation in a medium with no variation in porosity.

previous section, we presented a covariance function and associated power spectrum that can approximate the von Kàrmàn spectra as well as other spectra with shallower spectral exponents. This covariance function has four parameters that must be determined for a given sediment: the weighting exponent m, the covariance σ, and the upper and lower length scales, L_0 and L_1. One approach to determining these values is to find the best fit to the data as is typically done for propagation models based on grain contact friction or flow. This is necessary for the contact models since the measurable parameters required for these models remain largely unknown. Since the scattering loss model presented here relies on knowledge of the heterogeneity spectrum, we will proceed instead by considering a data set where this spectrum has been measured in addition to the necessary poroelastic parameters.

During SAX04 there was an extensive effort to measure sediment properties important to scattering from the seabed. As part of this effort, the sediment heterogeneity was measured

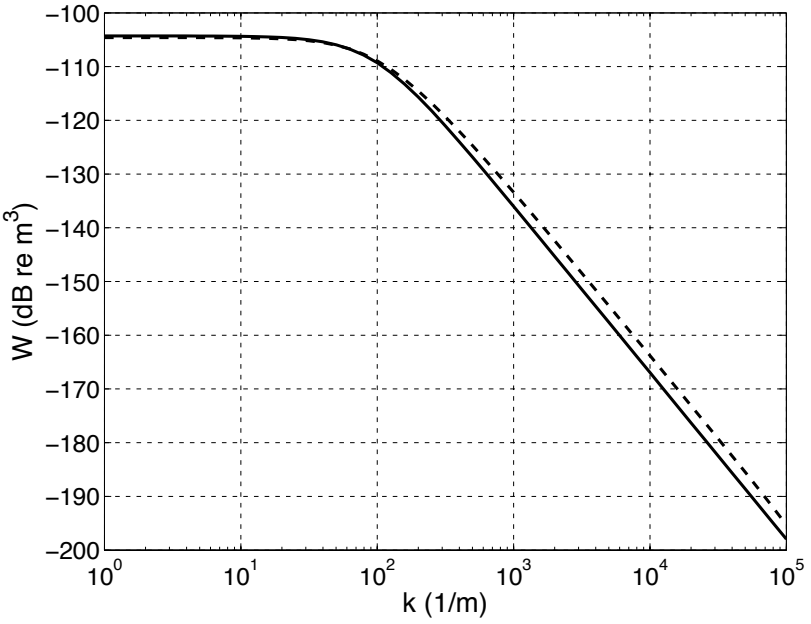

FIG. 6. The density fluctuation power spectrum measured during SAX04[17] (black line) and the approximate power spectrum determined using Eq. (79).

through the collection of diver cores and the deployment of a conductivity probe[17]. The diver cores were analyzed by either sectioning the cores and determining the porosity by measuring the wet and dry wet of each section or by mapping the density within the core with a computed tomography (CT) scanner. The conductivity probe was used to measure the formation factor in the sediment *in situ* which could then be used to determine the porosity. Each of these techniques were used to provide information about the density fluctuations at different scales in the sand sediment and, once sample size bias was corrected, it was possible to find a single power spectrum that incorporated each of these measurements.

While the conductivity probe deployment and the mass analysis of the diver cores were able to collect data on the porosity fluctuations directly, the data was converted into density fluctuations by application of Eq. (7) since this was the input required for scattering from the sediment. To apply these measurements to the EDFM perturbation wave equation, we must first convert the density fluctuation spectrum back into a spectrum for the porosity fluctuations. We will assume that the fluctuations in density determined using the CT

scanner were entirely due to fluctuations in porosity.

The power spectrum for the mean normalized density fluctuations was written as a von Kàrmàn spectrum,

$$W(\mathbf{k}) = \frac{w_3}{\left(k^2 + L^{-2}\right)^{\frac{\gamma_3}{2}}}, \tag{86}$$

where $w_3 = 2.0 \times 10^{-5}$ cm$^{-0.1}$, $\gamma_3 = 3.1$, and $L = 1.05$ cm. The porosity fluctuations can be related to the density fluctuations by

$$\delta\beta = \left(\frac{\partial\rho}{\partial\phi}\right)^{-1} \delta\rho \tag{87}$$

such that the variance becomes

$$\sigma_\beta^2 = \left(\frac{\partial\rho}{\partial\phi}\right)^{-2} \sigma_\rho^2. \tag{88}$$

Using Eq. (82), we can relate w_3 to the variance of the density fluctuations to find a coefficient of variation (CV). The CV is defined as the standard deviation divided by the mean and multiplied by 100. For the density fluctuations we find that the CV is 4.95%. Using Eq. (88) the CV for the porosity fluctuations is 16.31%.

With the relationship for the variance given by Eq. (88), the spectral strength for the porosity fluctuations becomes $w_{3\beta} = 5.07^{-5}$ m$^{-0.1}$ which corresponds to $\sigma^2 = (0.1631\beta_0)^2$ while the other spectral parameters remain unchanged. We can approximate this spectrum using the results of the previous section by choosing the upper limit of the integral to be $L_1 = L$. The value for weighting exponent can be determined using the approximate linear relation to find $m = \gamma_3 + 3$. The voxel size of the highest resolution CT data was 0.095 mm so the value for the lower limit of the integral will be chosen to be smaller then this voxel size, $L_0 = 10^{-5}$ m.

The approximate power spectrum using the parameters discussed above is compared to the true power spectrum in Fig. 6. Note that while the two spectra deviate at high wavenumbers and the approximation may be improved through a best fit to measured data, we will proceed with this approximation since it provides a means of deriving the parameters for the covariance function in Eq. (76) directly from the data.

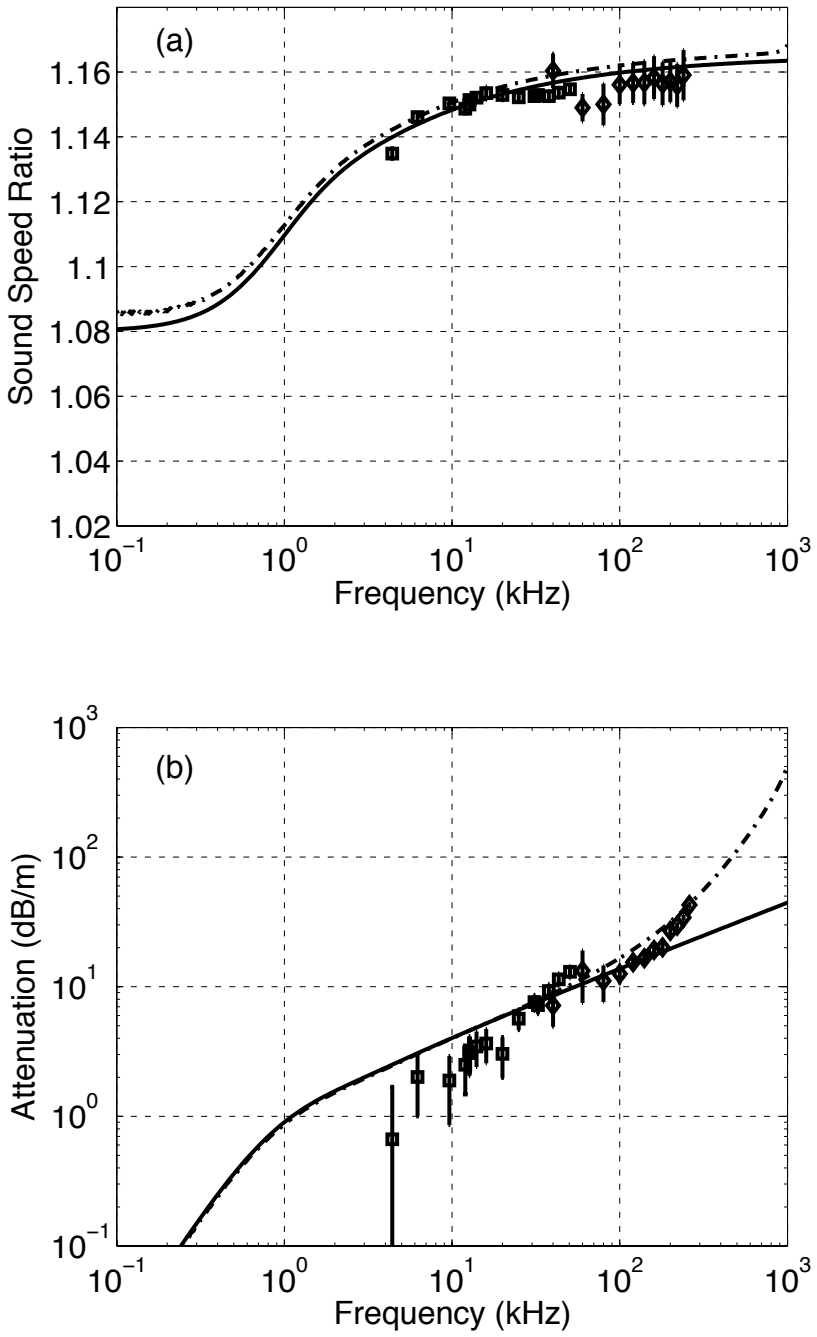

FIG. 7. The (a) sound speed ratio and (b) attenuation measured during SAX04 compared to the EDFM perturbation theory result (dash-dotted line) using the power spectrum for porosity fluctuations shown in Fig. 6 and the sediment parameters in Table I. Also shown is the unperturbed EDFM result (solid line). The markers correspond to the markers used by Hefner *et al.*[5] and the measurements are explained in detail there.

Using these parameters for the power spectrum (m, σ, L_0, and L_1), the sound speed and attenuation for the EDFM can be calculated using Eq. (59) and Eq. (84). Again the choice of the logrithmically spaced series approximation is improve convergence and for the calculations done here, $\delta = 0.1$. The results of the calculation are compared in Fig. 7 to the sound speed and attenuation measured during SAX04. For this calculation there are *no free parameters*. For the sound speed ratio, the relatively large CV produces a significant increase over the unperturbed result for all frequencies. This is due to the weakening of the medium as discussed in Section IV. Despite this increase, the model still captures the dispersion and matches the data.

The model also matches the attenuation data in the high-frequency regime where the measurements deviate from the unperturbed results. For this choice of m, the scattering contribution follows an $f^{0.8}$ dependence. While this is close to an f^1 dependence, the combination of the intrinsic and scattering contributions produce a net dependence that is less that f^1. This data set, however, does not follow a linear frequency dependence and this may be related to possible sorting and resettling of the sediment caused by the passage of Hurricane Ivan just prior to the start of the experiment.

VII. DISCUSSION

The sound speed and attenuation data coupled with the complete set of environmental measurements provided a unique opportunity to test the scattering loss mechanism. Unfortunately these opportunities are rare due to the range of measurements and the breadth of technical know-how required to collect that data. More often than not, a subset of the required sediment parameters are collected and the remaining unknowns are either chosen to conform to previous measured values or determined from a fit to the data. Likewise for measurements of heterogeneity which are often collected at length scales much larger then those required for the high-frequency propagation modeling presented here.

Despite this lack of knowledge, by incorporating scattering losses into the poroelastic

equations, we have constrained the model in a way that sets it apart from those based on grain contact dynamics. Heterogeneities in the sediment porosity that are large enough to produce significant scattering losses should also produce significant scattering from the sediment interface. This would mean that a fluctuation power spectrum that is chosen to fit a given sound speed and attenuation measurement should also fit measurements of sediment backscattering strength. For this comparison to be meaningful, there would have to be no other dominant scattering mechanisms such as shells or interface roughness. There are data sets available for this comparison and with the propagation theory on a firm footing[18], future work will focus on performing this type of comparison.

Another issue to be addressed is the need to solve the wave equations numerically. While the physics might be correctly captured, this introduces an additional complication when trying to apply this theory in other acoustic models or techniques when the heterogeneity statistics are an unknown parameter. This would be particularly true in remote sensing inversions where the scattering response of the sediment was used to determine key sediment properties. This suggests the need for approximations to the wave number solution that simplfy the application of the theory.

VIII. CONCLUSIONS

To explain the anomalous high-frequency attenuation observed in both ocean and laboratory sand sediments, we introduced scattering losses to Biot Theory and EDFM by applying perturbation theory. Unlike the previous study which found that heterogeneities in the bulk frame modulus were too weak to produce significant losses, small variations in the porosity can significantly increase the attenuation. While perturbation theory was applied to both Biot's poroelastic equations and the effective medium fluid model, the EDFM scattering result provides a good approximation to the full Biot Theory as it does for a homogeneous sand sediment. Since the integral in the scattering equations has an analytic solution for the exponential correlation function, a generalization of the exponential function was intro-

duced. This function can approximate both the von Kàrmàn correlation function as well as other functions whose associated power spectra have shallower spectral slopes. With this correlation function, the perturbation EDFM model can produce attenuation with frequency dependence which range from $f^{1/2}$ to $f^{5/2}$.

Using the sediment parameters and heterogeneity spectrum that were measured during SAX04, the sediment sound speed and attenuation predicted by the perturbation EDFM successfully models the data collected during the experiment. This model succeeds without any free parameters. While this data set is unique in that all of the necessary sediment properties were known, most measurements of sound speed and attenuation are not collected with collocated environmental measurements. The heterogenity statistics in these situations may be constrained by measurements of volume scattering from the sediment since the underlying physics are the same. Future work will explore this connection.

Acknowledgments

This research was supported by the Office of Naval Research.

References

[1] M. Kimura, "Velocity dispersion and attenuation in granular marine sediments: Comparison of measurements with predictions using acoustic models", J. Acoust. Soc. Am. **129**, 3544 (2011).

[2] K. Lee, E. Park, and W. Seong, "High frequency measurements of sound speed and attenuation in water-saturated glass-beads of varying size", J. Acoust. Soc. Am. **126**, EL28–EL33 (2009).

[3] K. L. Williams, D. Jackson, E. Thorsos, D. Tang, and S. Schock, "Comparison of sound speed and attenuation measured in a sandy sediment to predictions based on the Biot theory of porous media", IEEE J. Ocean. Eng. **27**, 413–428 (2002).

[4] B. T. Hefner and K. L. Williams, "Sound speed and attenuation measurements in unconsolidated glass-bead sediments saturated with viscous pore fluids", J. Acoust. Soc. Am. **120**, 2538–2549 (2006).

[5] B. Hefner, D. Jackson, K. L. Williams, and E. Thorsos, "Mid- to High-Frequency Acoustic Penetration and Propagation Measurements in a Sandy Sediment", IEEE J. Ocean. Eng. **34**, 372–387 (2009).

[6] N. P. Chotiros and M. Isakson, "A broadband model of sandy ocean sediments: Biot-Stoll with contact squirt flow and shear drag", J. Acoust. Soc. Am. **116**, 2011–2022 (2004).

[7] M. Buckingham, "On pore-fluid viscosity and the wave properties of saturated granular materials including marine sediments", J. Acoust. Soc. Am. **122**, 1486–+ (2007).

[8] B. T. Hefner and D. R. Jackson, "Dispersion and attenuation due to scattering from heterogeneities of the frame bulk modulus of a poroelastic medium", J. Acoust. Soc. Am. **127**, 3372–3384 (2010).

[9] B. T. Hefner, D. R. Jackson, and J. Calantoni, "The effects of scattering from heterogeneities in porosity during sound propagation through sand sediments.", J. Acoust. Soc. Am. **125**, 2746 (2009).

[10] K. L. Williams, "An effective density fluid model for acoustic propagation in sediments derived from Biot theory", J. Acoust. Soc. Am. **110**, 2276–2281 (2001).

[11] S. M. Rytov, Y. A. Kravtsov, and V. I. Tatarskii, *Principles of statistical radiophysics. 4. Wave propagation through random media.* (Springer-Verlag, Berlin) (1989).

[12] T. M. Müller and B. Gurevich, "A first-order statistical smoothing approximation for the coherent wave field in random porous random media", J. Acoust. Soc. Am. **117**, 1796–1805 (2005).

[13] J. Frank C Karal and J. B. Keller, "Elastic, Electromagnetic, and Other Waves in a Random Medium", Journal of Mathematical Physics **5**, 537–547 (1964).

[14] C. Jones, "High-frequency acoustic volume scattering from biologically active marine sediments", Ph.D. thesis, UNIVERSITY OF WASHINGTON (1999).

[15] C. Jones and D. Jackson, "Small perturbation method of high-frequency bistatic volume

scattering from marine sediments", IEEE J. Ocean. Eng. **26**, 84–93 (2001).

[16] M. Calvet and L. Margerin, "Velocity and attenuation of scalar and elastic waves in random media: A spectral function approach", J. Acoust. Soc. Am. **131**, 1843 (2012).

[17] K. B. Briggs, A. Reed, D. Jackson, and D. Tang, "Fine-Scale Volume Heterogeneity in a Mixed Sand/Mud Sediment off Fort Walton Beach, FL", IEEE J. Ocean. Eng. **35**, 471–487 (2010).

[18] B. T. Hefner and D. R. Jackson, "The role of porosity fluctuations in scattering from sand sediments and in propagation losses within the sediment.", The Journal of the Acoustical Society of America **126**, 2168–2168 (2009).

TABLE I. Parameters used in modeling SAX04 data[3]. The parameters chosen were determined from best fits of unperturbed Biot Theory to the data, but all parameters except the SAX04 porosity fall within the measurement uncertainties.

Parameter	SAX04
Porosity (β)	0.388
Mass density of sand grains (ρ_g)	2660 kg/m^3
Mass density of water (ρ_f)	1024 kg/m^3
Bulk modulus of sand grains (K_g)	3.2 $\times 10^{10}$ Pa
Bulk modulus of frame (K_b)	4.36 $\times 10^7$ Pa
Shear modulus of frame (μ_b)	2.92 $\times 10^7$ Pa
Bulk modulus of water (K_f)	2.40 $\times 10^9$ Pa
Viscosity (η)	0.00096 kg/m·s
Permeability (κ)	3.4 $\times 10^{-11}$ m^2
Tortuosity (α)	1.41

List of Figures

Measurement and modeling of sound propagation in a heterogenous sediment

Brian T. Hefner[1], Darrell R. Jackson[1]

[1]Applied Physics Laboratory, University of Washington, 1013 NE 40th Street, Seattle, WA 98105, USA {**hefner, drj**}**@apl.washington.edu**

A sand sediment is inherently heterogeneous due to the random packing of the sand grains. Measurements and simulations have shown that the random packing can lead to the formation of force chains and hence heterogeneities of the frame moduli. X-ray tomography also indicates the presence of pore structure heterogeneities which may lead to variations in the porosity and permeability of the sediment. Heterogeneities in any of these parameters can lead to scattering of the Biot fast compressional wave into incoherent fast, slow, or shear waves producing an increase in attenuation. In order to account for this loss, perturbation theory has been applied to Biot's poroelastic equations to develop a general theory of sound propagation in a randomly varying sand sediment. In this paper, the theory is applied to both bulk frame modulus and porosity heterogeneities. The implications of scattering loss on sound speed and attenuation measurements are also examined. In these measurements, the coherent and incoherent fields are typically present when autocorrelation or spectral techniques are used to process the data. The presence of the incoherent field may therefore lead to incorrect estimations of the sound speed and attenuation. (Work supported by the US Office of Naval Research).

1 Introduction

Over the last two decades, there has been an increasing interest in the physics of randomly packed granular materials. Research into these materials has uncovered a number of important consequences that follow from the random arrangements of the grains, particularly the formation of force chains[1] and the presence of local fluctuations in the density of the material[2]. While a majority of this research has focused on dry granular media, the results are equally applicable to saturated granular media such as a sand sediment. As a consequence of the random packing of the sand sediment, the presence of force chains should lead to heterogeneities in the bulk moduli of the sediment. The local density fluctuations should manifest in heterogeneities in the porosity, permeability, and tortuosity of the sediment since each of these parameters depend on the structure of the sediments pore space.

For a Biot medium, these heterogeneities can lead to scattering from a propagating fast Biot wave into incoherent fast, slow, and shear waves. This conversion of energy from the coherent field into incoherent will lead to an increase in the attenuation of the coherent field. This may explain the increased attenuation at high frequencies observed during the sediment acoustics experiments in 1999 (SAX99)[3] and 2004 (SAX04)[4] as well as in laboratory experiments[5]. By applying perturbation theory to Biot's poroelastic equations, wave equations have been developed which account for these scattering losses due to fluctuations in the frame bulk modulus or the porosity of the sediment.

The paper begins by briefly summarizing the application of perturbation theory to Biot's poroelastic equations. The predictions of the model for a heterogenous frame modulus are considered for both a sand sediment and a sintered glass bead medium. The model is then applied to sand sediment with a heterogenous porosity. The implications of this model for the measurement of attenuation are considered in the last section.

2 Perturbation Theory

A brief summary of the results of applying perturbation theory to Biot's poroelastic equations is given here while a detailed derivation can be found in [6]. The starting point for the theory are Biot's poroelastic equations consolidated into a single matrix equation as,

$$\nabla\left([\mathsf{K}]\,\nabla\cdot\mathbf{U}\right)-[\tilde{\mu}_0]\,\nabla\times(\nabla\times\mathbf{U})+[\rho_0]\,\omega^2\mathbf{U}=0, \quad (1)$$

where

$$[\mathsf{K}]=\begin{bmatrix} H & -C \\ C & -M \end{bmatrix} \quad (2)$$

is the matrix of Biot coefficients (see Ref. [3]),

$$[\rho]=\begin{bmatrix} \rho & -\rho_f \\ \rho_f & -\rho^* \end{bmatrix}, \quad (3)$$

is the density matrix,

$$[\tilde{\mu}]=\begin{bmatrix} \mu_b & 0 \\ 0 & 0 \end{bmatrix}, \quad (4)$$

is the frame shear modulus matrix, and

$$\mathbf{U}=\begin{bmatrix} \mathbf{u} \\ \mathbf{w} \end{bmatrix}, \quad (5)$$

is the displacement field of the solid frame $\mathbf{u}$ and the relative displacement of the pore fluid to the frame $\mathbf{w}=\beta\left(\mathbf{u}-\mathbf{u_f}\right)$. In the equations above, $\omega=2\pi f$ where f is the frequency, ρ_f is the density of the pore fluid, ρ_g is the sediment particle mass density, $\rho=(1-\beta)\,\rho_g+\beta\rho_f$ is the mean sediment density, β is the porosity,

$$\rho^*=\frac{\alpha\rho_f}{\beta}+\frac{iF\eta}{\kappa\omega}, \quad (6)$$

α is the tortuosity, κ is the permeability, η is the pore fluid viscosity, and the parameter F represents the deviation from Poiseuille flow as frequency increases. The expression for F is given and discussed in Ref. [3]. Note that the Biot coefficients depend on the frame bulk modulus, K_b, while both $[\mathsf{K}]$ and $[\rho]$ depend on the porosity.

We consider a poroelastic medium in which the sediment parameter of interest varies randomly with position. For example, for the frame bulk modulus,

$$K_b(\mathbf{r}) = K_{b0} + \delta K_b(\mathbf{r}), \tag{7}$$

where $K_{b0} = \langle K_b(\mathbf{r})\rangle$, $\delta K_b(\mathbf{r})$ is the local fluctuation of the bulk modulus, and $\langle \delta K_b(\mathbf{r})\rangle = 0$. To account for these random variations, we expand the matrices in Eq. (1) as a Taylor series about the mean value. Again, for the bulk modulus variation,

$$[\mathsf{K}] = [\mathsf{K}_0] + [\mathsf{F}_{b1}]\,\delta K_b + \frac{1}{2}[\mathsf{F}_{b2}]\,\delta K_b^2 + \ldots, \tag{8}$$

where $[\mathsf{K}_0]$ is the homogenous Biot coefficient matrix and

$$[\mathsf{F}_{bn}] = \frac{\partial^n [\mathsf{K}_0]}{\partial K_b^n}. \tag{9}$$

If the heterogenous poroelastic equation is rewritten as

$$\mathfrak{L}\cdot\mathbf{U} = 0, \tag{10}$$

substitution of the expanded expressions yields,

$$(\mathfrak{L}_0 + \mathfrak{L}_1 + \mathfrak{L}_2 + \ldots)\cdot\mathbf{U} = 0, \tag{11}$$

where $\mathfrak{L}_0\cdot\mathbf{U} = 0$ is the homogenous poroelastic equation. The displacement fields can be expanded as

$$\mathbf{U} = \langle\mathbf{U}\rangle + \mathbf{U_s}, \tag{12}$$

where $\langle\mathbf{U}\rangle$ is the mean coherent field and $\mathbf{U_s}$ is the incoherent, scattered field for which $\langle\mathbf{U_s}\rangle = 0$.

Substitution of Eq. (12) into Eq. (11), yields the expansion of the poroelastic equations,

$$\begin{aligned}\mathfrak{L}_0\cdot\langle\mathbf{U}\rangle &+ \mathfrak{L}_0\cdot\mathbf{U_s} + \mathfrak{L}_1\cdot\langle\mathbf{U}\rangle \\ &+ \mathfrak{L}_1\cdot\mathbf{U_s} + \mathfrak{L}_2\cdot\langle\mathbf{U}\rangle = 0,\end{aligned} \tag{13}$$

where we have neglected all terms higher than second order. Since $\langle\mathfrak{L}_1\rangle = 0$, the mean of Eq. (13) yields

$$\mathfrak{L}_0\cdot\langle\mathbf{U}\rangle + \langle\mathfrak{L}_1\cdot\mathbf{U_s}\rangle + \langle\mathfrak{L}_2\rangle\cdot\langle\mathbf{U}\rangle = 0. \tag{14}$$

Subtracting Eq. (14) from Eq. (13) and neglecting all terms higher than first order, we find the equation for $\mathbf{U_s}$ in terms of $\langle\mathbf{U}\rangle$,

$$\mathfrak{L}_0\cdot\mathbf{U_s} = -\mathfrak{L}_1\cdot\langle\mathbf{U}\rangle. \tag{15}$$

This equation can be solved using the poroelastic Green's tensor to yield the solution for $\mathbf{U_s}$,

$$\mathbf{U_s}(\mathbf{r}) = \int \mathfrak{G}(\mathbf{r},\mathbf{r}')\cdot\mathfrak{L}_1(\mathbf{r}')\cdot\langle\mathbf{U}(\mathbf{r}')\rangle\, d^3\mathbf{r}'. \tag{16}$$

Substituting this expression back into Eq. (14), we find the final equation for a poroelastic wave propagating through a heterogenous medium,

$$\begin{aligned}\mathfrak{L}_0(\mathbf{r}) &\cdot \langle U(\mathbf{r})\rangle \\ &+ \left\langle \mathfrak{L}_1(\mathbf{r})\cdot\int \mathfrak{G}(\mathbf{r},\mathbf{r}')\cdot\mathfrak{L}_1(\mathbf{r}')\cdot\langle\mathbf{U}(\mathbf{r}')\rangle\, d^3\mathbf{r}'\right\rangle \\ &+ \langle\mathfrak{L}_2(\mathbf{r})\rangle\cdot\langle\mathbf{U}(\mathbf{r})\rangle = 0.\end{aligned} \tag{17}$$

3 Bulk Modulus Variations

Application of Eq. (17) to the case of variations in the frame bulk modulus yields a wave equation for the medium which can be written as,

$$-([\mathsf{K}_{\mathsf{eff}}] - [\tilde{\mu}_0])\,\mathbf{k}(\mathbf{k}\cdot\mathbf{A}) - k^2[\tilde{\mu}_0]\,\mathbf{A} + [\rho_0]\,\omega^2\mathbf{A} = 0, \tag{18}$$

where the effective Biot coefficient is

$$\begin{aligned}[\mathsf{K}_{\mathsf{eff}}] &= [\mathsf{K}_0] \\ &- [\mathsf{F}_{b1}]\sum_{n=1}^{2}[\mathsf{G}_n][\mathsf{F}_{b1}]\,k_n^4 I_n \\ &- \left([\mathsf{F}_{b1}][\mathsf{K}_0]^{-1}[\mathsf{F}_{b1}] - \frac{1}{2}[\mathsf{F}_{b2}]\right)\sigma_{bb}^2,\end{aligned} \tag{19}$$

and

$$I_n = \frac{1}{k}\int_0^\infty \mathrm{e}^{ik_nR} C_{bb}(R)\sin(kR)\,dR. \tag{20}$$

In this perturbed wave equation, k_n is the unperturbed wave numbers where n = 1 and 2 is associated with the fast and slow wave respectively and

$$[\mathsf{G}_1] = \frac{[\mathsf{K}_0]^{-1} - [\rho_0]^{-1}\omega^{-2}k_2^2}{k_1^2 - k_2^2}, \tag{21}$$

$$[\mathsf{G}_2] = \frac{[\mathsf{K}_0]^{-1} - [\rho_0]^{-1}\omega^{-2}k_1^2}{k_2^2 - k_1^2}. \tag{22}$$

In Eq. (20), we have assumed that the variations in the modulus are statistically homogenous (spatially stationary) and isotropic so that the covariance of the modulus variations should depend only on the distance $R = |\mathbf{r} - \mathbf{r}'|$. Note also that $\sigma_{bb}^2 = C_{bb}(0) = \langle\delta K_b^2\rangle$ is the variance of the perturbation in the frame bulk modulus.

For the bulk modulus variations, there is scattering from the coherent fast wave into incoherent fast and slow waves and no scattering into incoherent shear waves. Also the coherent shear wave is unaffected by the bulk modulus variations.

Before considering results for a specific covariance function, some general properties of the the effective Biot coefficient matrix can be identified. When the variance of the perturbation goes to zero, the matrix reduces to the homogenous result, $[\mathsf{K}_0]$, as one would expect. The second term in Eq. (19) depends on the form of the covariance function and captures the effects of scattering on the coherent field. The third term does not depend on the frequency and scales only with

Parameter	SAX99 Sand	Sintered Glass Beads
β	0.385	0.37
ρ_g	2690 kg/m^3	2530 kg/m^3
ρ_f	1023 kg/m^3	1023 kg/m^3
K_g	3.2×10^{10} Pa	4.3×10^{10} Pa
K_b	4.36×10^{7} Pa	4.23×10^{9} Pa
μ_b	2.92×10^{7} Pa	7.94×10^{9} Pa
K_f	2.395×10^{9} Pa	2.395×10^{9} Pa
η	0.00105 kg/m·s	0.00105 kg/m·s
κ	2.5×10^{-11} m^2	4.43×10^{-11} m^2
α	1.35	1.60

Table 1: Parameters used in the examples.

the variance of the perturbation. This is the softening of the medium due to the modulus variations and leads to a decrease in sound speed over all frequencies. This is discussed in more detail in the Appendix of Ref. [6].

The theory given in Eq. (1) accounts for only the second-order scattering contributions to the mean propagating field. For large fluctuations in the medium, it may be necessary to account for higher-order scattering contributions. To determine whether it is necessary to account these contributions, we follow the approach of Rytov[7] and use an iterative method to estimate the contribution of a subset of the higher-order scattering contributions (this is discussed in detail in Ref. [6]). The condition which must be met is that the contribution of this higher correction to the wavenumber be small compared to the second order correction to the wavenumber, which can be expressed as

$$\frac{\left|k^{(2)} - k\right|}{|k - k_1|} \ll 1, \tag{23}$$

where k is the wavenumber determined from Eq. (18) and $k^{(2)}$ is determined using the iterative method discussed in Ref. [6]. Note also that, although an analytic proof of causality is not possible, the examples below have been found to satisfy a numerically integrated, twice-subtracted dispersion relation.

To determine whether variations in the frame bulk modulus are sufficient to account for the high-frequency attenuation observed in sand sediments, we will consider predictions of the model using the exponential covariance function,

$$C_{bb}(R) = \sigma_{bb}^2 e^{-R/L}, \tag{24}$$

for which the integral in Eq. (20) can be solved to yield,

$$I_n = \frac{\sigma_{bb}^2}{\left(L^{-1} - ik_n\right)^2 + k^2}, \tag{25}$$

where L is the characteristic length scale of the bulk modulus variations. Note that the wavenumber which we wish to determine is in the denominator of Eq. (25). To solve Eq. (18), we will approximate the wavenumber in the denominator of the integral by the unperturbed wavenumber, k_n.

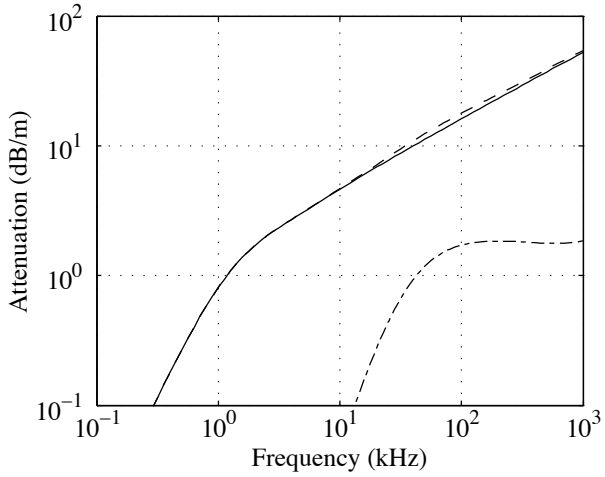

(a)

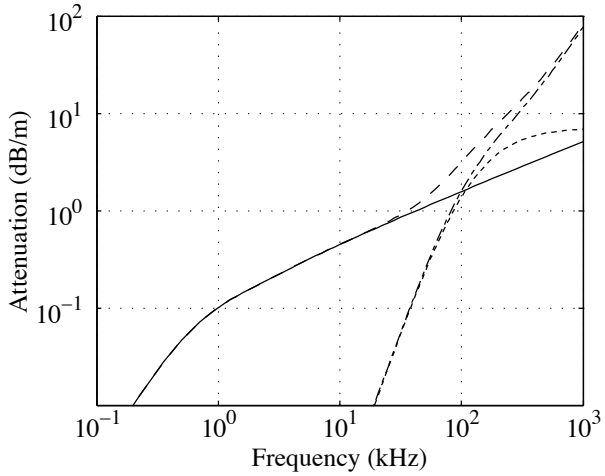

(b)

Figure 1: Examples of attenuation for a medium with frame bulk modulus variations and sediment parameters corresponding to (a) SAX99 sand sediment and (b) sintered glass beads. For the SAX99 sediment, $L = 1$ mm and $\sigma_{bb}^2 = 0.73K_b^2$. For the sintered glass beads, $L = 1.6$ mm and $\sigma_{bb}^2 = 0.14K_b^2$. In each plot, the unperturbed attenuation (solid line), the attenuation with scattering (long dashed line), the attenuation contribution due to fast and slow wave scattering (dash-dot line), and the attenuation contribution due slow wave scattering only (short dashed line) are shown. For the SAX99 sediment, the attenuation with scattering comes entirely from fast to slow wave scattering.

In the examples given here, two media will be considered: the SAX99 sand sediment and a sintered glass bead pack. The sediment parameters for these media are given in Table 1 and, as can be seen in the table, the most significant difference in the material parameters is the magnitude of the frame moduli. The bulk and shear frame moduli for the sintered glass bead pack are two orders of magnitude larger than those of the SAX99 sediment.

The attenuation determined by solving Eq. (18) using the

parameters in Table 1 is shown in Figure 1. In these plots, the contribution due to scattering into fast and slow waves was determined by subtracting the attenuation when $\sigma_{bb}^2 = 0$ from predicted attenuation. The contribution to attenuation from fast to slow wave scattering was also determined by setting $[\mathsf{G}_1] = 0$ and subtracting the unperturbed attenuation from slow wave only scattering prediction. For the SAX99 sediment, the values for L and σ_{bb}^2 were chosen to show an increase in attenuation in the region where the attenuation measured during SAX99 begins to deviate from Biot theory. In order to get even this slight increase, the standard deviation of the bulk modulus variations had to be increased to $\sigma_{bb} = 0.83K_b$ and, as a result, the condition in Eq. (23) has been violated.

For the sintered glass beads, scattering creates a significant increase in attenuation at high frequencies for a modest choice of σ_{bb}^2 and the condition given in Eq. (23) is satisfied. In the SAX99 sediment, the attenuation was due to scattering from the coherent fast wave into incoherent slow waves. For the glass beads, the slow wave scattering dominates initially but as the frequency increases, the scattering into incoherent fast waves becomes the dominant loss mechanism.

4 Porosity Variations

The perturbation solution given in Eq. (17) has also been solved for a medium with varying porosity,

$$\beta(\mathbf{r}) = \langle\beta\rangle + \delta\beta(\mathbf{r}), \tag{26}$$

where $\langle\delta\beta(\mathbf{r})\rangle = 0$. In this case, both $[\mathsf{K}]$ and $[\rho]$ depend on the porosity and each must be expanded as a Taylor series. With these expansions, the resulting wave equation has a more complicated form than was found for the bulk modulus variations and hence will not be given here. In contrast to bulk modulus result, the variations in porosity lead to scattering from the coherent fast wave into incoherent fast, slow, and shear waves. The coherent shear wave is also affected by scattering losses, however we will only considered fast wave propagation here.

An example of the attenuation due to porosity variations is shown in Figure 2 again assuming an exponential covariance function. In this example $L = 2.5$ mm and $\sigma_{bb} = 0.18\beta$ and for these a condition similar to Eq. (23) is satisfied. Causality has also been numerically confirmed. As opposed to the bulk modulus variation results, the attenuation is dominated by fast wave scattering. The onset of fast wave scattering produces a transition from the $f^{0.5}$ dependence predicted to by Biot theory to an f^2 dependence at very high frequencies. In the transition, the attenuation is approximately linear consistent with the frequency dependence observed in the SAX99 data. This indicates that while the bulk modulus in a sand sediment is too weak to produce significant scattering, fluctuations in parameters for which Biot theory is more sensitive, such as porosity, may be able to account for the increased attenuation observed in sand sediments.

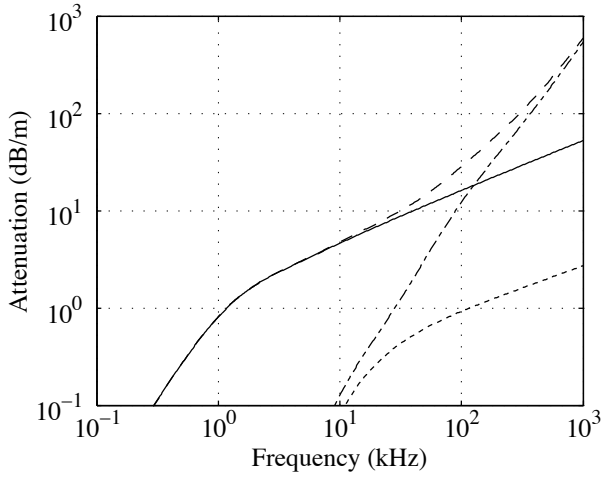

Figure 2: Example of attenuation for a medium with porosity variations and sediment parameters corresponding to the SAX99 sand sediment. In this example, $L = 2.5$ mm and $\sigma_{bb}^2 = 0.03\beta^2$. The unperturbed attenuation (solid line), the attenuation with scattering (long dashed line), the attenuation contribution due to fast and slow wave scattering (dash-dot line), and the attenuation contribution due slow and shear wave scattering only (short dashed line) are shown.

Since the scattering is dominated by the fast wave scattering, it is possible to approximate the perturbed poroelastic wave equation by applying perturbation theory to the effective density fluid model (EDFM)[8]. In the EDFM, the frame moduli are set to zero and

$$H = C = M = \left(\frac{(1-\beta)}{K_g} + \frac{\beta}{K_f}\right)^{-1}. \tag{27}$$

This leads to a significant simplification of the poroelastic equations and simplifies the perturbation theory solution as well.

The dominance of the fast wave scattering also suggests a connection between sound propagation within the sediment and the scattering of sound from the sediment interface. For sound incident above the critical grazing angle, heterogeneities within the sediment can produce significant backscattering (See [9] and references therein). Typically, perturbation theory is used to predict this scattered field and, since the sediment is treated as a fluid model, compressional wave scattering is assumed to dominate. The dominance of fast compressional wave scattering in the propagation models discussed here suggests that the mechanism responsible for the increased attenuation may also be responsible for volume scattering from the sediment. Experiments have recently been conducted in order to study this hypothesis.

5 Implications for Measurements

If scattering from the coherent fast wave into incoherent slow waves were the dominant attenuation mechanism, the incoherent energy would be quickly dissipated due to the

high attenuation of the slow wave. Since this is not the case, the incoherent fast waves can have a significant effect on a single signal transmitted between two points in the sediment. These effects were seen in the SAX99 measurements (see Figure 5 in [3]) and to a lesser extent in the SAX04 and laboratory measurements. The complications that these effects cause in model/data comparisons can be eliminated by determining the mean field from a number of measurements at different locations within the sediment. The perturbation result in Eq. (17) predicts the wavenumber for this mean field.

As opposed to determining the mean field through multiple measurements in the sediment, the sound speed and attenuation are usually calculated for each measurement location and then the mean of those values are determined. How these mean values relate to the values modeled using Eq. (17) is unclear. To illustrate this, we will consider how these different techniques affect the value for attenuation determined using the procedure outlined in Ref. [10].

In this procedure, an array consisting of a source and two receivers, each at a different distance from the source, are inserted into the sediment and a pulse is transmitted and recorded. The array is removed from the sediment and reinserted at a different location. This continues until a large number of locations are sampled. To determine the attenuation, the received pulses are carefully windowed and and filtered to isolate the first six cycles of the received pulse. The spectral amplitudes at the frequency of interest are determined and the ratio of these amplitudes becomes

$$A_g(\omega) = \left| \frac{P_{1g}(\omega)}{P_{2g}(\omega)} \right|^2, \tag{28}$$

where $P_{1g}(\omega)$ and $P_{2g}(\omega)$ are the spectral amplitudes at the far and near receivers respectively. A similar ratio, A_w, is taken for a set of pulses taken with the same array in the water column. The attenuation is then determined from the ratio of these spectral ratios,

$$\alpha = \frac{1}{2d} \ln\left(\frac{A_w}{A_g}\right), \tag{29}$$

where d is the difference in the distances between each receiver and the source.

To determine the attenuation of the coherent field, the mean of the pulses received at each location on each receiver would be used in Eq. (28) to determine what we will call the coherent ratio A_{g0}. The attenuation of the coherent field is then

$$\alpha_0 = \frac{1}{2d} \ln\left(\frac{A_w}{A_{g0}}\right). \tag{30}$$

When the spectral ratio is determined at each location, we will assume that the affect of the incoherent field can be captured as

$$A_{gi} = A_{g0} + \delta A_{gi}, \tag{31}$$

where the index i denotes the location at which the measurement was taken. We will also assume that $\langle \delta A_{gi} \rangle = 0$. Substitution of A_{gi} into Eq. (28) and assuming $\delta A_{gi} \ll A_{g0}$ yields the attenuation at location i,

$$\alpha_i = \frac{1}{2d} \ln\left(\frac{A_w}{A_{g0}}\right) - \frac{1}{2d}\frac{\delta A_{gi}}{A_{g0}} + \frac{1}{4d}\frac{\delta A_{gi}^2}{A_{g0}^2}. \tag{32}$$

and the mean attenuation of all the locations becomes

$$\langle \alpha_i \rangle = \alpha_0 + \frac{1}{4d}\frac{\langle \delta A_{gi}^2 \rangle}{A_{g0}^2}. \tag{33}$$

The mean attenuation is biased upward relative to the attenuation of the coherent field.

6 Conclusions

Perturbation theory has been applied to Biot's poroelastic equation to develop a wave equation which captures scattering losses within the sediment up to second order. The theory has been applied to sediments with heterogeneities in the frame bulk modulus and the porosity. For a sand sediment, the frame modulus is too weak to produce scattering and hence attenuation at levels observed in experiments such as SAX99. When porosity variations are present, significant scattering can occur for modest levels of variation and in this case, the scattering loss is dominated by scattering from the coherent field into incoherent fast compressional waves. This suggests that applying perturbation theory to the EDFM may successfully capture the observed attenuation while simplifying the resulting theory.

The implications of the scattering model were also considered in the context of attenuation measurements. While a simple example was used to illustrate the types of issues that can arise when comparing data and models, a more careful analysis of the effects of scattering on measurement of sound speed and attenuation in the sediment is required.

7 Acknowlegdements

This work was supported by the US Office of Naval Research.

References

[1] C. Liu, S.R. Nagel, D.A. Schecter, "Force fluctuations in bead packs," *Science* 269, 513-515 (1995)

[2] A.V. Anikeenko, N.N. Medvedev, "Structural and entropic insights into the nature of the random-close-packing limit," *Phys. Rev. E* 31101 (2008)

[3] K. L. Williams, D. R. Jackson, E. I. Thorsos, D. Tang, S. G. Schock, "Comparison of sound speed and attenuation measured in a sandy sediment to predictions based on the Biot theory of porous media," *IEEE J. Ocean. Eng.* 27, 413–428 (2002)

[4] B. T. Hefner, D. R. Jackson, K. L. Williams, and E. I. Thorsos, "Mid- to High-Frequency Acoustic Penetration and Propagation Measurements in a Sandy Sediment," *IEEE J. Ocean. Eng.* 34, 327–387 (2009)

[5] B. T. Hefner, K. L. Williams,"Sound speed and attenuation measurements in unconsolidated glass-bead sediments saturated with viscous pore fluids," *J. Acoust. Soc. Am.* 120, 2538–2549 (2006)

[6] B. T. Hefner, D. R. Jackson,"Dispersion and attenuation due to scattering from heterogeneities of the frame bulk modulus of a poroelastic medium," *J. Acoust. Soc. Am.* 127, 3372–3384 (2010)

[7] S. M. Rytov, Y. A. Kravtsov, V. I. Tatarskii, *Principles of Statistical Radiophysics* (Springer, Berlin, 1989), Vol. 4.

[8] K. L. Williams, "An effective density fluid model for acoustic propagation in sediments derived from Biot theory," *J. Acoust. Soc. Am.* 110, 22762281 954 (2001)

[9] D. R. Jackson and M. D. Richardson, *High-Frequency Seafloor Acoustics* (Springer, New York, 2006)

[10] M. J. Buckingham, M. D. Richardson, "On tone-burst measurements of sound speed and attenuation in sandy marine sediments," *IEEE J. Ocean. Eng.* 27, 429–453 (2002)

High frequency measurements of backscattering from heterogeneities and discrete scatterers in sand sediments

Brian T. Hefner[1], Darrell R. Jackson[1], Anatoliy N. Ivakin[1], Dajun Tang[1]

[1]Applied Physics Laboratory, University of Washington, 1013 NE 40th Street, Seattle, WA 98105, USA, {**hefner,drj,ivakin,djtang**}**@apl.washington.edu**

In an effort to study the importance of heterogeneities and discrete inclusions, a series of backscattering measurements were made on a sand sediment in a fresh water test pond. Backscattering was measured at frequencies from 200 to 500 kHz as a function of grazing angle. In order to reduce the role of roughness, the sediment was artificially smoothed by divers. The residual roughness was characterized by a laser line scanner and found to be insufficient to account for the observed backscattering. The sediment has a very narrow grain size distribution with very few large shell fragments or other inclusions. This indicates that the predominant scattering mechanism is volume scattering due to the presence of heterogeneities in the sediment. The backscattering measurements are compared to the predictions of perturbation theory for a heterogenous sediment. The role of larger, discrete scatterers was also examined by the careful addition of a layer of shell fragments to the surface of the sediment.

1 Introduction

It has generally been assumed that the roughness of the water/sediment interface is the dominant cause of backscattering from sandy ocean sediments. For sand sediments, measurements such as those made by Williams[1] and Greenlaw[2] have brought this assumption into question for scattering above 100 kHz and these results indicate that a second scattering mechanism may dominate at these frequencies. Subsequent measurements made during SAX04[3] and in the laboratory[4] have since supported this conclusion.

A likely candidate for this high frequency scattering mechanism is volume scattering, either from heterogeneities in the sediment properties, from large scatterers such as shells and shell hash, or from the sand grains themselves. Testing volume scattering models which incorporate these types of scatterers relies on the proper characterization of the heterogeneities and particles in the sediment as well as the characterization of competing mechanisms such as roughness. This can be difficult, especially in an ocean environment where the complexity of the environment requires both spatial and temporal measurements of the relevant parameters.

Figure 1: Eight element high frequency array mounted on the APL mobile tower.

In order to overcome these difficulties, a series of measurements of backscattering from a sand sediment were conducted in a man-made, fresh water pond. The pond is sheltered from both weather events and the effects of bioturbation. Working in this evironment made it possible to manipulate the sediment interface to reduce the effects of roughness scattering and carefully characterize the sediment properties. This paper discusses those experiments and highlights some of the preliminary results of the data analysis.

2 Measurements

The experiments were performed in the Spring of 2009 and 2010 in the Naval Surface Warfare Center (NSWC) test facility in Panama City, Florida. This facility includes a man-made, fresh water pool that is approximately 12 m deep and has a sand sediment bottom which is 1.5 m deep. The sand sediment bottom is approximately 50 m long and 30 m wide. The water at the facility is treated to maintain visibility (up to 10 m), to discourage the growth of algae and other plant life, and to keep the environment free of fish.

In the NSWC facility, the Applied Physics Laboratory (APL) deployed the bottom mounted rail and mobile tower system which had previously been deployed for the Sediment Acoustics Experiment 2004 (SAX04)[1]. The rail consists of three sections, each 7 m in length, for a total length of 21 m. The tower is mounted on the rail and can move either continuously or incrementally during data acquisition. A number of acoustic systems can be deployed with the tower for synthetic aperture sonar, forward scattering, and acoustic backscattering measurements.

This paper focuses on backscattering measurements made

using three pairs of piston sources mounted on the tower (Fig. 1). This array of source/receiver pairs allowed backscattering from the sand sediment to be measured from 200 to 500 kHz. The array itself was used previously with the tower during SAX04. For the pond experiment, however, the tower was reconfigured such that the array could be mounted at the base of the tower, either 0.5 m or 1.0 m above the sediment. This allowed the grazing angle to be varied from 7° to 80°. In order to obtain backscattering from multiple realizations of the sediment, the tower was moved at 2 cm increments over a 2 m long section of the rail for scattering from a total of 100 independent realizations of the bottom.

In order to reduce the effects of roughness scattering, a section of the sediment interface, 2.5 m wide and extending 4.5 m from the front edge of the rail, was smoothed by divers. This process involved placing two metal flats on either side of the field, both leveled and at equal height, and pulling a third metal flat edge along the top of the metal flats, scraping the sand interface smooth. Sand was added and removed during this process to ensure that the entire area was smoothed and leveled without any large holes.

To confirm that the area was flat and to determine any residual roughness, the interface height was measured with a laser line scanner mounted on the in-situ measurement of porosity (LLS-IMP2) system[5]. This system is capable of measuring the sediment elevation with sub-millimeter accuracy over a 0.30 m by 3.5 m area. The horizontal resolution of the system is 1 mm. In addition to measuring to the sediment elevation, the system also captures the (uncalibrated) reflectivity of the sediment at each measurement point allowing the user to visually identify objects on the interface such as shells or vegetation.

The sound speed and attenuation in the sediment was measured using the sediment transmission measurement system (STMS1) "attenuation array,"[6] which was previously deployed in SAX99 and SAX04. This system consists of two sources and two receivers which divers insert into the sediment. The sound speed and attenuation is then measured approximately 10 cm below the sediment interface from 40-280 kHz. Diver cores were also collected for bulk sediment density and porosity. Several of these cores were preserved for computed tomography (CT) analysis to be performed by the Naval Research Laboratory at Stennis Space Center (NRL-SSC)[7]. This analysis should allow us to quantify the density variations in the sediment as well as any distribution in grain sizes. Previous particle size analysis found that the mean grain size for this sediment was 0.25 mm with a very narrow distribution of sizes about this mean.

The sand in the test facility has very few shells or large particles. In order to study how shells may contribute to scattering from the sediment, a set of backscattering measurements were also made on a smoothed sand interface on which a random distribution of shells pieces was placed. These shell pieces were created by breaking larger shells and keeping only those shell pieces whose largest dimension was between 0.5 and 1 cm. Each shell piece was approximately 0.4 cm thick. The shells were distributed on the smooth sediment interface by dropping 1600 pieces along a 0.5 m by 2 m area such that each 0.5 m by 0.5 m area had 400 pieces (Figure 2). The long axis of this area is perpendicular to the rail. After the backscatter data was collected, a layer of sand was deposited and smoothed such that the shells were flush buried. Backscatter was again measured to examine how the scattering changed.

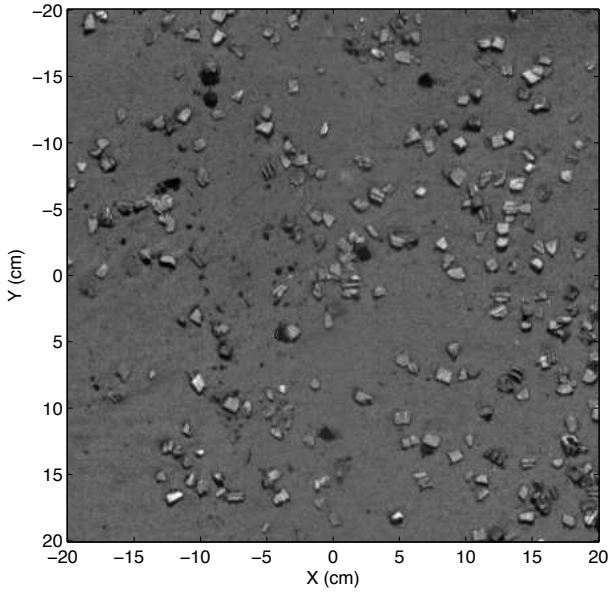

Figure 2: Surface reflectivity collected by the LLS-IMP2 of the diver-smoothed interface with the shells distributed on the surface.

3 Scattering from Smooth Sediment

The backscattering strength measured for the smoothed surface is shown in Figure 3 for 200, 300, 400 and 500 kHz. At this time, only the data for grazing angles below 60° has been processed. Also shown in the plots is the prediction of perturbation theory for the scattering due to the residual roughness measured using the LLS-IMP2. For the smoothed interface, the roughness spectra in the region of interest was fit using a power law[1] with $\gamma_2 = 2.32$ and $w_2 = 2.73 \times 10^{-9}$ m$^{4-\gamma_2}$. This seems to capture the scattering up to the critical angle for all but the highest frequencies. The data collected by the LLS-IMP2 does not extend to the wave numbers required for the high frequencies and the power law is extrapolated into this region. It may be possible however to improve the processing of the laser data to extend the spectra into this region.

Above the critical angle, the data is much higher than the roughness perturbation theory prediction and indicates that there is a different scattering mechanism at these angles. Since the CT scans of the diver cores have not been processed, the data was fit using a small-perturbation fluid volume scattering model. The spectrum chosen for an eyeball fit of the data was a von Karman spectrum for the den-

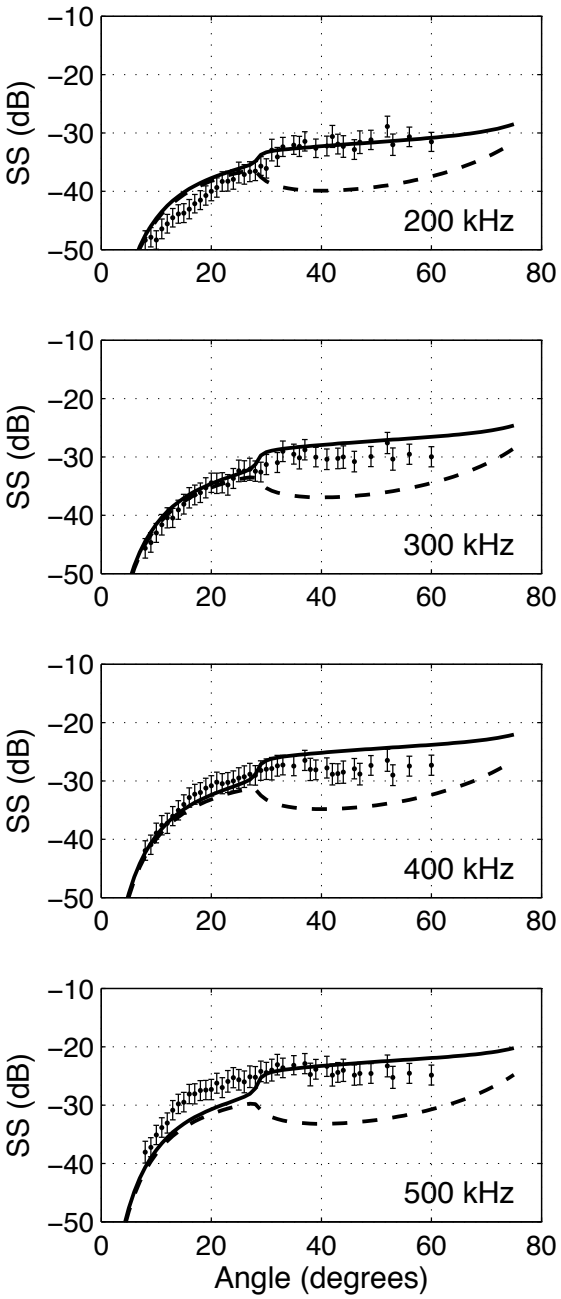

Figure 3: Backscattering strength from the diver-smoothed sand surface. The roughness scattering (dashed line) was calculated using the fluid small-roughness perturbation approximation using the roughness spectrum measured with the LLS and the measured sediment properties. The volume scattering (solid line) was determined using a spectrum for density fluctuations determined from a fit to the data.

sity fluctuations with $\gamma_3 = 3.225$, $w_3 = 0.001$ m^3, and $L_3 = 0.0002$ m. This is a very small characteristic length and is on the order of the grain size in the medium. Note that this is only a preliminary fit of the data. A proper model/data comparison will involve the heterogeneity spectrum determined from the CT scans and will also need to take into account the poroelastic nature of the sediment through either

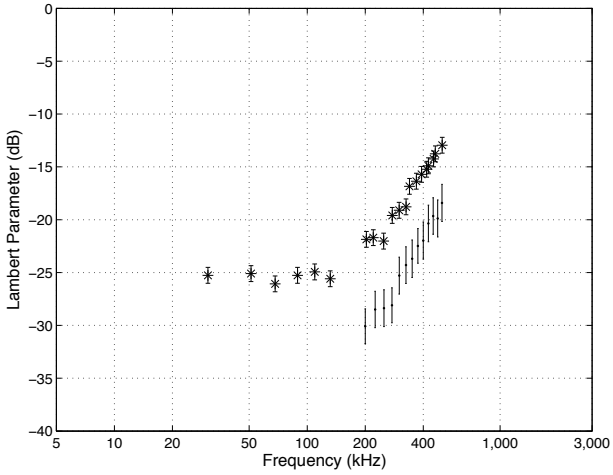

Figure 4: Lambert parameter as a function of frequency for the diver-smoothed sand surface (points) for a grazing angle of 30° grazing. Also plotted are the SAX04 data (astricks) for comparison.

the Biot model or the effective density fluid model[8].

The Lambert parameter, determined by dividing the backscattering cross section by $\sin^2(\theta)$[3], is shown for $\theta = 30°$ in Figure 4. Since this array was used during SAX04, the Lambert parameter determined for the SAX04 data is also shown for comparison. Both the current data for a clean sand sediment and the SAX04 data for an ocean sediment follow a similar frequency dependence, while the current data is roughly 5 dB lower than the SAX04 data.

4 Scattering from a Shell Layer

The backscattering strength for the shells distributed on the smoothed sediment is shown in Figure 5 for 200, 300, 400 and 500 kHz. The 2 m long area that the shells were distributed over made it possible to collect scattering data from the shells from $\theta = 12°$ to $\theta = 40°$. Also shown in these plots is the backscattering strength for the 1 m wide smoothed sediment next to the shell area. Diver cores were collected following the measurements discussed in the previous section and the sediment was smoothed again for this experiment. This smoothed data was collected as a control to confirm that the sediment response did not change between manipulations.

The presence of the shell pieces significantly increases the backscattering strength relative to the smoothed interface. The backscattering strength is relatively constant as a function of grazing angle with little or no difference between the data above and below the critical angle. Below the critical grazing angle, there is very little change in the backscattering strength over the frequency band of the measurements (200–500 kHz). Above the critical angle, there is a slight increase at the high end of the frequency band (>400 kHz) as can be seen in the Lambert parameter plotted in Figure 6. Note also that the scattering levels for the smoothed sed-

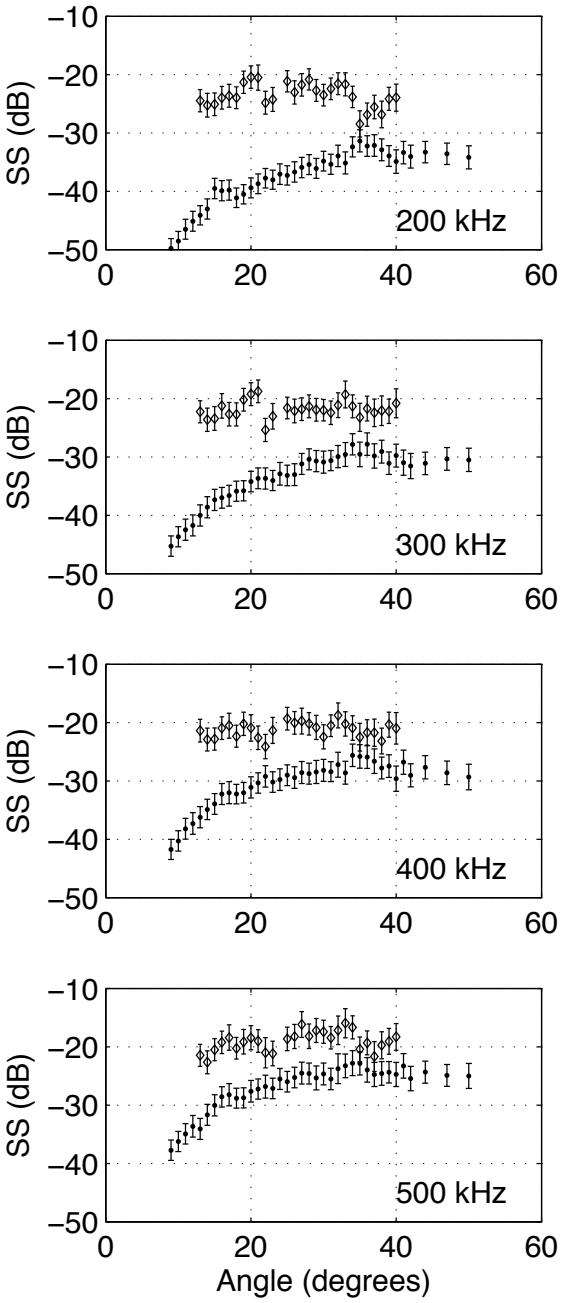

Figure 5: Backscattering strength for the diver-smoothed sand surface with shells (open diamonds) and without shells (solid circles).

iment did not differ appreciably for the two manipulations.

5 Conclusions

In the experiments in the NSWC test facility, it was possible to reduce the roughness of the sand sediment to levels such that above critical grazing roughness does not explain the observed scattering. A second scattering mechanism can be clearly seen to dominate. These measurements in conjunction with sediment characterization including CT scans of sediment samples should allow us to test volume scattering theories. The increase in backscattering due to the presence of shell fragments indicates their importance in high frequency scattering.

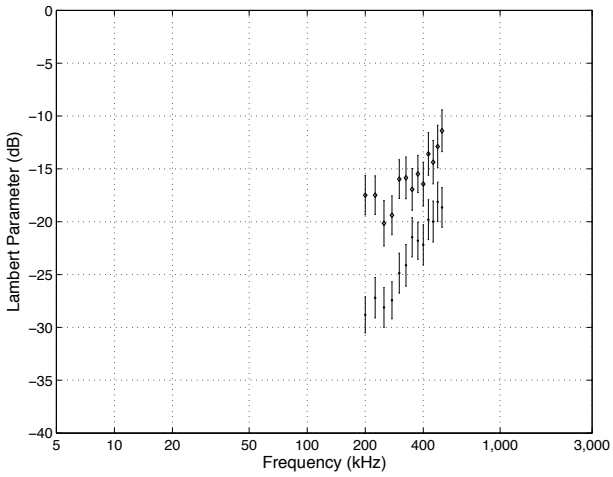

Figure 6: Lambert parameter as a function of frequency for the diver-smoothed sand surface (solid circles) and the proud shell layer (open circles).

6 Acknowledgements

This work was supported by the US Office of Naval Research.

References

[1] K. L. Williams, D. R. Jackson, E. I. Thorsos, D. Tang, K. B. Briggs, "Acoustic backscattering experiments in a well characterized sand sediment: Data/model comparisons using sediment fluid and Biot models," *IEEE J. Ocean. Eng.* 27, 376–387 (2002)

[2] C. F. Greenlaw, D. V. Holliday, D. E. McGehee, "High-frequency scattering from saturated sand sediments," *J. Acoust. Soc. Am.* 115, 2818-2823 (2004)

[3] K. L. Williams, D. R. Jackson, D. Tang, K. B. Briggs, E. I. Thorsos, "Acoustic backscattering from a sand and a sand/mud environment: Experiments and data/model comparisons," *IEEE J. Ocean. Eng.* 34, 388–399 (2009)

[4] A. N. Ivakin, J.-P. Sessarego, "High frequency broad band scattering from water-saturated granular sediments: Scaling effects," *J. Acoust. Soc. Am.* 122, EL165-EL171 (2007)

[5] C.-C. Wang, D. Tang, "Seafloor roughness measured by a laser line scanner and a conductivity probe," *IEEE J. Ocean. Eng.* 34, 459–465 (2009)

[6] B. T. Hefner, D. R. Jackson, K. L. Williams, and E. I. Thorsos, "Mid- to High-Frequency Acoustic Penetration and Propagation Measurements in a Sandy Sediment," *IEEE J. Ocean. Eng.* 34, 327–387 (2009)

[7] A. H. Reed, K. B. Briggs, D. L. Lavoie, "Porometric properties of siliciclastic marine sand: A comparison of traditional laboratory measurements with image analysis and effective medium modeling," *IEEE J. Ocean. Eng.* 27, 581–592 (2002)

[8] K. L. Williams, "An effective density fluid model for acoustic propagation in sediments derived from Biot theory," *J. Acoust. Soc. Am.* 110, 22762281 954 (2001)

Proceedings of the 11th European Conference on Underwater Acoustics

POWER-LAW ATTENUATION DUE TO SCATTERING FROM POROSITY HETEROGENEITIES IN SANDY SEDIMENTS

BT Hefner Applied Physics Laboratory, University of Washington, Seattle, WA, USA
DR Jackson Applied Physics Laboratory, University of Washington, Seattle, WA, USA

1 INTRODUCTION

Measurements in sandy sediments in both the laboratory [1] and the ocean [2, 3] have found that the attenuation at high frequencies ($>$10 kHz) follows a linear frequency dependence. While this is consistent with Hamilton's original observations [4], the sound speed dispersion follows that predicted by Biot for a porous medium [2]. Theories that have been developed to explain this behavior have typically focused on the unconsolidated nature of the sand and postulated that there is loss at the grain contacts due to friction or fluid motion [5, 6]. Models that incorporate grain contact friction into Biot theory essentially introduce a dashpot into the frame moduli with a frequency response that produces the appropriate frequency dependence in the attenuation. While the parameters that are necessary to describe the dashpot are related to the properties of the medium, such as the fluid viscosity, these parameters are instead determined from a best fit to the data. At this point in their development, the theories have limited predictive power and there is not a clear relationship between the model parameters and the material properties.

An alternative theory has recently been proposed to explain the measured dispersion and attenuation which does not invoke any loss mechanism at the grain contacts but instead considers the inherently random nature of the granular packing. This random packing should produce heterogeneities in the sediment properties which in turn should cause sound propagating through the material to be scattered. A coherent acoustic wave passing through the material should lose energy to this scattering mechanism and have an increased attenuation relative to that predicted by Biot Theory. This scattering mechanism has been modeled by applying perturbation theory to Biot's poroelastic equations [7]. Heterogeneity in the bulk frame modulus was initially considered as a likely candidate to produce scattering loss. However it was found that due to the unconsolidated nature of the medium, the bulk frame modulus was too weak to produce sufficient scattering. Attention has since shifted to variations in the porosity, a property that has a strong influence on the sound propagation through the medium [2].

For this scattering mechanism, the model predicts that the form of the correlation function, or alternatively the power spectral density, for the porosity variations determines the frequency dependence of the attenuation. For the commonly used Von Karman correlation function [8], the resulting frequency dependence remains below f^1 as the Hurst coefficient, ν, is varied over the range $0 < \nu \leq 1$. For the special case of $\nu = 1/2$, the Von Karman correlation function reduces to the exponential correlation function which produces an attenuation that goes as f^2 then rolls off at high frequencies. In this paper, we determine the form of the correlation function that produces the observed attenuation.

2 PERTURBATION THEORY

In order to examine how the choice of correlation function affects the frequency dependence of attenuation, we will consider the sediment as a fluid medium with heterogeneities in the porosity. To model the scattering loss, we will apply perturbation theory to the heterogenous wave equation,

$$\nabla \cdot \left(\frac{1}{\rho} \nabla p \right) + \omega^2 \kappa p = 0, \tag{1}$$

where ρ is the density, κ is the compressibility, and $\omega = 2\pi f$. We will assume that both the density and the compressibility are functions of the porosity which varies as a function of position,

$$\beta(\mathbf{r}) = \beta_0 + \delta\beta(\mathbf{r}), \tag{2}$$

where $\beta_0 = \langle \beta(\mathbf{r}) \rangle$ is the average over an ensemble of realizations of the medium (denoted by $\langle \cdot \rangle$), $\delta\beta(\mathbf{r})$ is the local fluctuation of the porosity, and $\langle \delta\beta(\mathbf{r}) \rangle = 0$. To account for the random variations in porosity, we will expand both the density and compressibility as Taylor series about the mean porosity,

$$\kappa(\mathbf{r}) = \kappa_0 \left(1 + F_\kappa \delta\beta(\mathbf{r})\right), \tag{3}$$

where

$$F_\kappa = \frac{1}{\kappa_0} \frac{\partial \kappa_0}{\partial \beta}, \tag{4}$$

and

$$\frac{1}{\rho(\mathbf{r})} = \frac{1}{\rho_0} \left(1 - F_\rho \delta\beta(\mathbf{r}) + \frac{1}{2} F_\rho^2 \delta\beta(\mathbf{r})^2 + ...\right), \tag{5}$$

where

$$F_\rho = \frac{1}{\rho_0} \frac{\partial \rho_0}{\partial \beta}. \tag{6}$$

For both the compressibility and the density, we have assumed that all higher derivatives are equal to zero.

Substituting these expansions into Eq. 1, we can write the expanded equation of motion as,

$$\left(L_0 + L_1(\delta\beta) + L_2\left(\delta\beta^2\right)\right) p = 0, \tag{7}$$

where $L_0 p = 0$ is the homogenous equation of motion. We can now solve this equation by using the perturbation solution for propagation through a heterogenous medium [7],

$$L_0(\mathbf{r})\, p_0(\mathbf{r}) + \left\langle L_1(\mathbf{r}) \int g_0(\mathbf{r}, \mathbf{r}')\, L_1(\mathbf{r}')\, p_0(\mathbf{r}')\, d^3\mathbf{r}' \right\rangle + \langle L_2(\mathbf{r}) \rangle\, p_0(\mathbf{r}) = 0, \tag{8}$$

where

$$g_0(\mathbf{r}, \mathbf{r}') = \frac{\mathrm{e}^{ik_0|\mathbf{r}-\mathbf{r}'|}}{4\pi|\mathbf{r}-\mathbf{r}'|} \tag{9}$$

is the Green's function for a point source in a homogenous medium. Eq. (8) was first derived by Karal and Keller for propagation of acoustic, elastic, and electromagnetic waves through heterogenous media [9].

After some manipulation and assuming a plane wave solution for the mean field in the medium,

$$p_0 = A\mathrm{e}^{i\mathbf{k}\cdot\mathbf{r}}, \tag{10}$$

the equation for the effective wavenumber in the medium is

$$\begin{aligned} k^2 &- k_0^2 - k_0^4 F_\kappa^2 \int g_0(R) C(R) \mathrm{e}^{-i\mathbf{k}\cdot\mathbf{R}} d^3\mathbf{R} + 2ik_0^2 F_\rho F_\kappa \int \mathbf{k}\cdot\nabla g_0(R) C(R) \mathrm{e}^{-i\mathbf{k}\cdot\mathbf{R}} d^3\mathbf{R} \\ &- F_\rho^2 \int \mathbf{k}\cdot\nabla\nabla' g_0(R)\cdot\mathbf{k}\, C(R) \mathrm{e}^{-i\mathbf{k}\cdot\mathbf{R}} d^3\mathbf{R} + \frac{1}{2} F_\rho^2 \sigma^2 k^2 = 0, \end{aligned} \tag{11}$$

where $C(\mathbf{R}) = \langle \delta\beta(\mathbf{r})\, \delta\beta(\mathbf{r}') \rangle$ is the covariance, $\mathbf{R} = \mathbf{r} - \mathbf{r}'$, and $\sigma^2 = C(0)$ is the variance of the porosity fluctuations. This equation can also be expressed in terms of the power spectrum of the porosity variations,

$$W(k) = \frac{1}{(2\pi)^3} \int C(R)\, e^{i\mathbf{k}'\cdot\mathbf{R}} d^3\mathbf{R}, \tag{12}$$

as

$$\begin{aligned} k^2 &- k_0^2 - k_0^4 F_\kappa^2 (2\pi)^3 \int \frac{W(\mathbf{k}-\mathbf{k}')}{k'^2 - k^2} d^3\mathbf{k}' - 2i(2\pi)^3 k_0^2 F_\rho F_\kappa \int \mathbf{k}\cdot\mathbf{k}' \frac{W(\mathbf{k}-\mathbf{k}')}{k'^2 - k^2} d^3\mathbf{k}' \\ &+ (2\pi)^3 F_\rho 1^2 \int (\mathbf{k}\cdot\mathbf{k}')^2 \frac{W(\mathbf{k}-\mathbf{k}')}{k'^2 - k^2} d^3\mathbf{k}' + \frac{1}{2} F_\rho 2\sigma^2 k^2 = 0. \end{aligned} \tag{13}$$

If the covariance is the exponential function,

$$C(R) = \sigma^2 \mathrm{e}^{-R/L}, \tag{14}$$

where L is the characteristic length scale of the porosity heterogeneities, the integrals in Eq. (11) can be solved exactly.

3 THE VON KARMAN CORRELATION FUNCTION

One of the more commonly used covariance functions is the Von Karman covariance function which has the corresponding power spectrum,

$$W_v(k) = \frac{\sigma^2 L^3 \Gamma\left(\nu + \frac{3}{2}\right)}{\pi^{\frac{3}{2}} \Gamma(\nu) \left(1 + k^2 L^2\right)^{\nu + \frac{3}{2}}}, \tag{15}$$

where $0 < \nu \leq 1$. When $\nu = 0.5$, this power spectrum reduces to that of the exponential function,

$$W_e(k) = \frac{\sigma^2 L^3}{\pi^2 \left(1 + k^2 L^2\right)^2}. \tag{16}$$

In Fig. 1, the sound speed and attenuation were calculated for a sand sediment using the Von Karman covariance function when $\nu = 0.12$ and $\nu = 0.5$. For this example, the sediment density is $\rho = 2.0\ \mathrm{g/cm^3}$, the water sound speed is $c_w = 1500\ \mathrm{m/s}$, the sediment sound speed is $c_s = 1.1\, c_w$, and the ratio of the imaginary to real, unperturbed sediment wavenumber is $\delta = 0.0018$. The wavenumber ratio in a sand sediment is typically an order of magnitude larger than the value used here, but since we are considering scattering as the dominant loss mechanism in the sediment, we have chosen a lower value for the intrinsic attenuation.

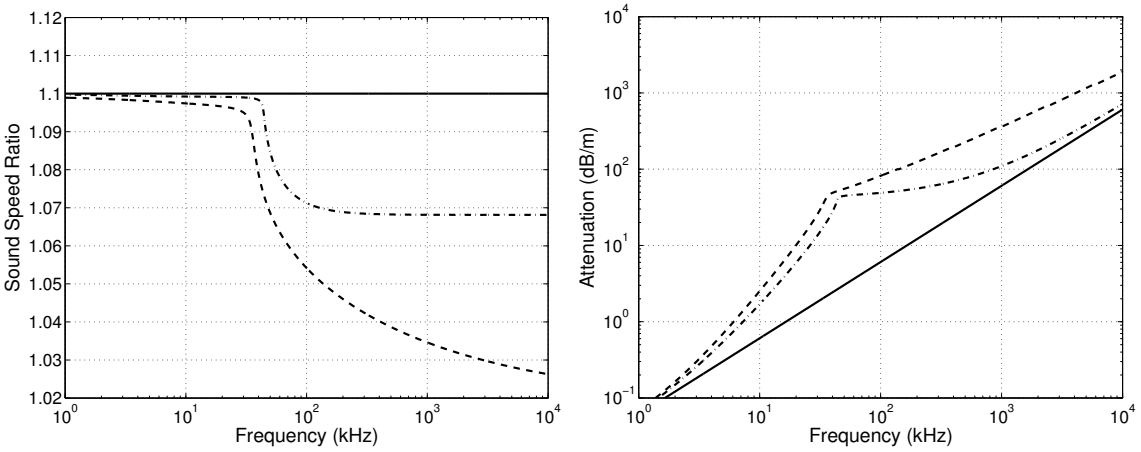

Figure 1: Sound speed ratio (left) and attenuation (right) solutions to the perturbation equation given in Eq. (8). In both both cases the Von Karman correlation function was used with $\nu = 0.5$ (dashed line) and $\nu = 0.12$ (dashed-dotted line). For both cases, $\sigma = 0.05$ and $L = 10$ cm. Also shown is the unperturbed solution (solid line).

In the examples, both covariance functions yield negative dispersion with the larger value for ν leading to a larger decrease in sound speed. For the attenuation, both covariances produce attenuations which follow an f^2 dependence below 40 kHz. At roughly 40 kHz, both attenuations exhibit a "knee" above which the scattering contribution due to the exponential covariance becomes constant while the contribution from the Von Karman with $\nu = 0.12$ follows an approximately $f^{0.5}$ dependence. Neither function yields the linear frequency dependence seen in both laboratory and ocean sand sediments.

For the power spectra given in Eqs. (15) and (16), as ν decreases the high wavenumber dependence of the spectra increases from k^{-4} for $\nu = 0.5$ to k^{-3} as ν approaches 0. As ν decreases, the frequency dependence of the attenuation increases from f^0 towards $f^{1/2}$. This indicates that in order to achieve a linear frequency dependence, the power spectrum should should follow a power-law, k^γ, where $\gamma > -3$. The difficulty with this form of the power spectrum is that if $\gamma \geq -3$ as $k \to \infty$, the variance, which is found by integrating over the power spectrum, diverges and the spectrum becomes non-physical.

4 CONSTRUCTING AN ARBITRARY COVARIANCE

While it is not possible to use a power law spectrum that has $\gamma > -3$ as $k \to \infty$, it is possible to construct a spectrum that follows the required power law over a limited band of k. This approach is similar to the Nearly Constant Q (NCQ) model developed originally for seismology [10]. In the NCQ model, the attenuation is modeled as a sum of relaxation mechanisms each of which has the same amplitude but different central frequencies. This produces a linear attenuation over the band in which these central frequencies reside.

To produce the spectra of interest here, we will write the covariance as a sum of exponential covariance functions,

$$C_\Sigma(R) = \sigma^2 \sum_{n=0}^{N} w_n e^{-\frac{R}{L_n}}, \tag{17}$$

where the correlation lengths are distributed logarithmically in size,

$$L_n = L_0 10^{n\Delta}, \tag{18}$$

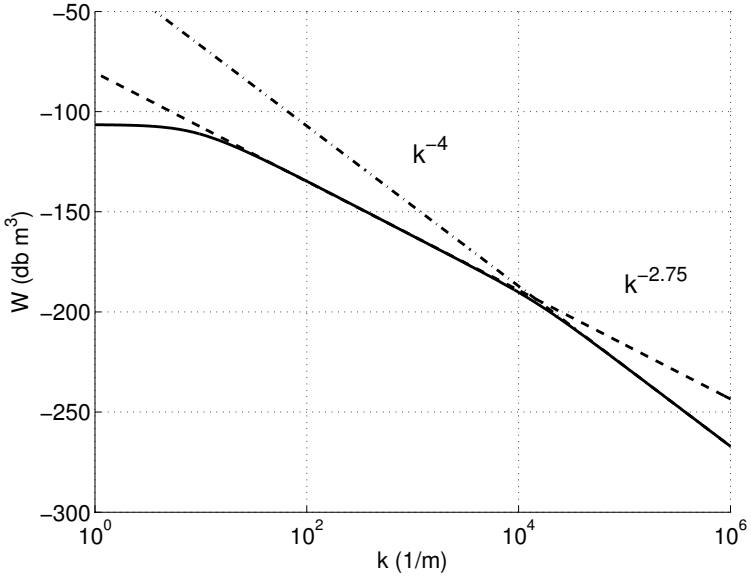

Figure 2: Power spectrum calculated using Eq. (21) with $\tau = -0.25$, $L_0 = 10$ cm, $L_N = 0.1$ mm, $\Delta = 0.1$, and $\sigma = 0.01$.

the density of the correlation lengths is determined by the spacing, Δ, the weight of each covariance is proportional to the correlation length raised to some power,

$$w_n = \frac{L_n^\tau}{\sum_{n=0}^{N} L_n^\tau}, \tag{19}$$

and

$$\sum_{n=0}^{N} w_n = 1. \tag{20}$$

This last relation insures that the covariance is equal to the variance at $R = 0$. The associated power spectrum can also be written as a sum of power spectra,

$$W_\Sigma(k) = \frac{\sigma^2}{\pi^2} \sum_{n=0}^{N} \frac{w_n L_n^{-3\tau}}{\left(k^2 + L_n^{2\tau}\right)^2}. \tag{21}$$

An example power spectrum constructed using this summation is shown in Fig. 2. For this example, $\tau = -0.25$ and the correlation lengths vary between $L_0 = 10$ cm, $L_N = 0.1$ mm.

5 MODELING LINEAR ATTENUATION

In applying this covariance summation, if $\tau > 0$ the slope of the spectrum in the wavenumber band of the summation corresponds to the von Karman spectrum and varies from $\gamma = -4$ to $\gamma = -3$. For negative values of τ, the spectral slope increases until $\tau = -4$ and $\gamma = 0$. To obtain a linear attenuation for the fluid model that we are considering here, $\tau = -0.25$. This value was used in Fig. 2 and also to calculate the attenuation and sound speed in Fig. 3.

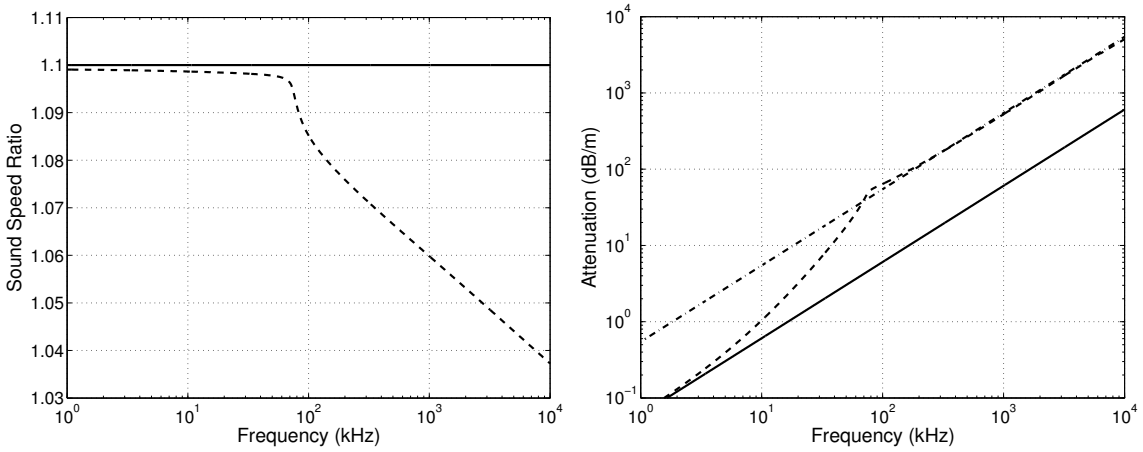

Figure 3: Sound speed ratio (left) and attenuation (right) calculated for the covariance given in Eq. (17) with $\tau = -0.25$, $L_0 = 10$ cm, $L_N = 0.1$ mm, $\Delta = 0.1$, and $\sigma = 0.01$. The solid lines are the unperturbed sound speed and attenuation, the dashed lines are the perturbation theory result, and the dash-dotted line is the attenuation for the unperturbed medium when $\delta = 0.0165$.

Note that while the attenuation follows a linear frequency dependence quite well, the sound speed shows significant negative dispersion which is not seen in most laboratory and ocean sand sediments. The fluid model is only an approximation used here to present both the perturbation theory and to show how a linear attenuation can be obtained. A better approximation to a sand sediment can be found by applying perturbation theory to the effective density fluid model (EDFM) [11]. Again Eq. (17) can be applied and a linear attenuation can be obtained with $\tau = -1$ which produces a spectral slope of $\gamma = -2$. In this case the sound speed exhibits weak, positive dispersion at high frequencies that is more consistent with measurements.

6 CONCLUSION

To account for heterogeneities in the porosity of a sand sediment, perturbation theory was applied to a fluid model of the sediment. The resulting wave equation shows negative dispersion and an increase in attenuation. For the commonly used Von Karman covariance function, the frequency dependence of the attenuation was less than that observed in most sand sediments. By using a sum of exponential covariance functions, it is possible to construct a covariance which can produce an attenuation with an arbitrary frequency dependence. It is therefore possible to obtain a linear attenuation with perturbation theory using this summation. While the resulting sound speed exhibits a dispersion which is greater than that observed in real ocean sediments, preliminary results indicate that this is not the case if perturbation theory is applied to EDFM.

ACKNOWLEDGEMENTS

This work was supported by the US Office of Naval Research.

REFERENCES

1. B. T. Hefner and K. L. Williams. Sound speed and attenuation measurements in unconsolidated glass-bead sediments saturated with viscous pore fluids. *J. Acoust. Soc. Am.*, 120(5): pp. 2538–2549, 2006.

2. K. L. Williams, D. Jackson, E. Thorsos, D. Tang, and S. Schock. Comparison of sound speed and attenuation measured in a sandy sediment to predictions based on the Biot theory of porous media. *IEEE J. of Ocean. Eng.*, 27(3): pp. 413–428, 2002.

3. B. Hefner, D. Jackson, K. L. Williams, and E. Thorsos. Mid- to High-Frequency Acoustic Penetration and Propagation Measurements in a Sandy Sediment. *IEEE J. of Ocean. Eng.*, 34: pp. 372–387, 2009.

4. E. L. Hamilton. Geoacoustic modeling of the sea floor. *J. Acoust. Soc. Am.*, 68(5): pp. 1313–1340, 1980.

5. N. P. Chotiros and M. Isakson. A broadband model of sandy ocean sediments: Biot-Stoll with contact squirt flow and shear drag. *J. Acoust. Soc. Am.*, 116: pp. 2011–2022, October 2004.

6. M. Buckingham. On pore-fluid viscosity and the wave properties of saturated granular materials including marine sediments. *J. Acoust. Soc. Am.*, 122: pp. 1486–1501, 2007.

7. B. T. Hefner and D. R. Jackson. Dispersion and attenuation due to scattering from heterogeneities of the frame bulk modulus of a poroelastic medium. *J. Acoust. Soc. Am.*, 127(6): pp. 3372–3384, 2010.

8. D. Jackson and M. Richardson. *High-Frequency Seafloor Acoustics*. Springer, New York, NY, 2006.

9. J. Frank C Karal and J. B. Keller. Elastic, Electromagnetic, and Other Waves in a Random Medium. *J. Math. Physics*, 5(4): pp. 537–547, 1964.

10. H. LiU, D. Anderson, and H. Kanamori. Velocity dispersion due to anelasticity; implications for seismology and mantle composition. *Geophys. J. R. Astron. Soc.*, 47(1): pp. 41–58, 1976.

11. K. L. Williams. An effective density fluid model for acoustic propagation in sediments derived from Biot theory. *J. Acoust. Soc. Am.*, 110(5): pp. 2276–2281, 2001.

PUBLICATIONS

1. Hefner, B.T. and D.R. Jackson (2013), “Attenuation in Sand Sediments Due to Scattering from Porosity Fluctuations,” in preparation for J. Acoust. Soc. Am.
2. Tang, D., and B.T. Hefner (2012), “Modeling interface roughness scattering in a layered seabed for normal-incident chirp sonar signals,” J. Acoust. Soc. Am. 131, EL302-EL308.
3. Hefner, B.T. and D.R. Jackson (2010), “Power-law attenuation due to scattering from porosity heterogeneities in sandy sediments,” in European Conference on Underwater Acoustics 2012.
4. Hefner, B.T., D.R. Jackson, A.N. Ivakin, and D. Tang (2010), “High frequency measurements of backscattering from heterogeneities and discrete scatterers in sand sediments,” in European Conference on Underwater Acoustics 2010.
5. Hefner, B.T. and D.R. Jackson (2010), “Measurement and modeling of sound propagation in a heterogeneous sediment,” in European Conference on Underwater Acoustics 2010.